Reinforced concrete beams strengthened with SRP/SRG systems: Experimental investigation

Annalisa Napoli[a], Roberto Realfonzo[a]*

[a] University of Salerno, Department of Civil Engineering, Via Giovanni Paolo II 132, 84084 Fisciano (SA), Italy
*Corresponding author

This is a post-peer-review, pre-copyedit version of an article published in Construction and Building Materials

The final authenticated version is available online at:

http://dx.doi.org/10.1016/j.conbuildmat.2015.06.027

REINFORCED CONCRETE BEAMS STRENGTHENED WITH SRP/SRG SYSTEMS: EXPERIMENTAL INVESTIGATION

Annalisa Napoli, Roberto Realfonzo*

Department of Civil Engineering, University of Salerno
Via Giovanni Paolo II, 132, 84084 Fisciano (SA), Italy

ABSTRACT

Steel reinforced polymer (SRP) and steel reinforced grout (SRG) have emerged as promising and cost-effective technologies for the external strengthening of RC structures.

Although the first studies date back to 2004, so far the literature related to the flexural strengthening of RC slab/beams with steel tapes is rather limited. As a result, the application of such materials on a real structural member may be discouraged and, conversely, the use of carbon/glass FRP alternative systems may be preferred.

The study presented in this paper contributes to filling this knowledge gap by presenting the results of 10 four-point bending tests performed on RC slabs strengthened with SRG/SRP systems. Test results have provided valuable information in terms of maximum forces, deformability and failure modes by varying number of layers and density of the steel tape. In particular, it has been shown that, disregarding the nature of the matrix (inorganic or polymeric), the presence of the external strengthening significantly increased the flexural strength of slabs, with percentage increases over the control (unstrengthened) member ranging from a minimum value of 27%, when using a single layer of low density tape, to a maximum of 106% in the case of SRP system with one layer of high density sheet.

Preliminary analytical studies were also performed in order to investigate the possibility of extending to the SRP/SRG systems the applicability of formulations currently reported in some national and international guidelines for the flexural strengthening of RC members with FRP sheets.

Keywords: Epoxy; Experimental tests; Flexural strengthening, Grout; Steel tapes; Strain; Strength.

---

* Corresponding author. Phone (+39) 089-964085. Fax (+39) 089-968739. *E-mail address:* rrealfonzo@unisa.it

1. Introduction

Over the years, the use of Fiber Reinforced Polymer (FRP) materials for the strengthening of reinforced concrete (RC) structural members has met an increasingly widespread consensus at both the academic and industrial levels, representing today a competitive alternative to traditional techniques.

In the case of external strengthening, it is well known that behind the FRP terminology, systems employing carbon fibers are typically referred to, whereas fewer applications make use of glass or aramid fibers. The successful application of such composites in the civil engineering has also been recognized through the spread of specific guidelines around the world, such as the Italian Guidelines CNR-DT 200 R1 [1] and the American Guidelines ACI 440.2R [2].

However, the growing interest in the composites industry towards the development of innovative and low cost solutions has led to the introduction of new techniques for the structural reinforcement that make use of other fibers in lieu of the carbon or glass ones. Among the "new generation" materials, the class of composites made of steel fiber sheets has emerged as one of the most promising and cost-effective solutions for external strengthening of RC members.

The steel tape consists of high carbon steel cords made by twisting steel wires within a micro-fine brass or galvanized coating; it can be in situ applied via wet lay-up by using epoxy resin or inorganic matrix, thus obtaining strengthening systems known with the acronym of SRP ("*Steel Reinforced Polymer*") and SRG ("*Steel Reinforced Grout*"), respectively. The tape can be required according to different densities (generally denoted as low, medium or high), depending on the number of wires distributed in the sheet width.

Although the first studies date back to 2004 [3,4], so far the scientific papers dealing with the use of steel fiber composites for the strengthening of RC structural members (due to bending, shear, or confinement deficiencies) are rather limited, as well as specific guidelines have not been published yet. As a result, the lack of an extensive knowledge on the applicability of these materials might guide the designer toward the choice of "proven" strengthening solutions or more marketed composite systems, i.e., those employing the above mentioned carbon or glass fibers.

By focusing on the flexural strengthening of RC beams/slabs with steel fiber materials, the bibliography reports the main papers by authors contributing to provide some information about the effectiveness of using SRP/SRG systems in the structural rehabilitation [3-15]. In particular, the experimental studies

performed by Wobbe et al. [3], by Prota et al. [5], by Kim et al. [6] and Balsamo et al. [9], are pointed out. Wobbe et al. [3] just performed a first experimental study devoted to prove the potential of the SRP/SRG technology in improving the performance of RC members.

In addition to highlight the influence of using different tape densities on the specimens' response, Prota et al. also investigated the flexural behaviour of beams strengthened with SRG sheets mechanically anchored to the concrete substrate by using nail anchors. It was shown that such nails do not improve the performance of the steel tape impregnated with cementitious grout, being the used tape of unidirectional type, as generally commercialized in the market; in fact, lacking a transverse link, the distribution of the local stress concentration at anchor location was not allowed; as a result, the subsequent bearing failure of nails was unable to improve the bond and delay the tape debonding [5].

Kim et al., instead, examined the efficiency of the SRP system by varying the width of the employed tape and the beneficial role played by the use of U-shape SRP wraps as end anchorages to prevent the peeling-off failure of the external reinforcement at the beam's intrados [6]. It was again proven the positive contribution of the SRP reinforcement in increasing the flexural capacity of RC beams; also, it was shown that the U-wraps improve the flexural stiffness by controlling diagonal crack width and providing anchorages to the longitudinal SRP sheets, which reduces their slip.

Finally, a comparative analysis of different composite material systems (CFRP-SRP-SRG) for the flexural strengthening of prestressed RC beams was performed by Balsamo et al. [9]; in that work, the convenience into using steel fiber sheet with respect to the carbon ones was verified, since a lower amount of materials and, thus, minor costs allow for obtaining similar effectiveness to CFRP systems in terms of maximum loads.

A few papers also report preliminary considerations regarding the theoretical prediction of the bending moment of RC beams strengthened with SRP at ultimate and service loads [6,11]. Conversely, a more detailed study is highlighted on the numerical simulation of the load-displacement behaviour of SRP/SRG strengthened beams [12], whereas the behaviour under serviceability conditions of SRP/SRG strengthened RC beams tested by Prota et al. [5] was deepened by Ceroni and Pecce [13]. These authors evidenced: a) the comparable behaviour between SRP and CFRP strengthened RC members, when characterized by equivalent amount of external reinforcement, and b) the more deformability exhibited by members strengthened with SRG sheets with respect to those upgraded with SRP.

Finally, some field applications have been also performed. In particular, an experimental study performed by Casadei et al. [14], explored the efficiency of the SRP systems in increasing the flexural strength of "double T" prestressed RC beams which were extracted from a decommissioned two-storey parking garage.

Lopez et al. [15], instead, proved that the application of the SRP strengthening to a concrete bridge structure has the potential to be a reliable and relatively easy-to-install technique; also they pointed out that the design procedure for SRP systems is comparable to that suggested by the Guide ACI 440 for FRP materials in force in 2007 [16]. In this regard, it can be reasonable to assume that the failure of an RC member strengthened with adhesively bonded steel fiber system, independently on the type of matrix (epoxy or cementitious), is attributable to concrete crushing (when the ultimate concrete compressive strain is reached) or to the failure of the composite system; the latter, in turn, can be due to the rupture of the fibers in tension or to the debonding mechanism which abruptly occurs with the detachment of more or less large concrete thickness. Therefore, the effectiveness of SRP/SRG systems in increasing the flexural response of RC members may significantly depend, from one side, on the bond behaviour at the concrete/reinforcement interface (that is mostly related to the matrix type) and, from the other side, on the efficiency of the used matrix (mainly the inorganic one) to impregnate the steel fabric.

With the aim to better focus on these two key aspects, the experimental study presented in this paper contributes to increase the current knowledge on the flexural behaviour of RC members strengthened with steel fiber sheets. In particular, the work deeply analyzes the results of 10 four-point bending tests performed on RC slabs strengthened with galvanized steel fiber tapes applied by using epoxy resin (SRP system) or thixotropic mortar (SRG system).

The main study parameters were: the number of layers (1 or 2); the different density of the steel tape (denoted as low, medium or high); the typology of reinforcement's application (from the top, by turning upside the slabs, or from the bottom, by placing them on a scaffold).

Test results have provided valuable information in terms of maximum forces, specimens' deformability, measured strains and curvatures which, coupled with the observed failure modes, are fundamental for a subsequent definition of an accurate design procedure for RC beams/slabs strengthened with SRP/SRG systems. To this purpose, it is highlighted that the bending tests presented herein are part of a wider experimental campaign also including several bond tests performed on SRG/SRP sheets adhesively

connected to concrete blocks; such tests, whose results are under publication, will allow for a more specific evaluation of the concrete/SRG (or SRP) interface behaviour, on which only few papers are actually available in literature [6,17,18].

The experimental evidence has also allowed for verifying the good performance of the SRG systems, whose effectiveness was not reduced by applying the strengthening system from the bottom, i.e., after having placed two slabs on a scaffold (at an height of about 1.80 m from the floor), in order to simulate the typical working operations found in the field.

Finally, preliminary analytical studies were performed to investigate the possibility of extending to the SRP/SRG systems the applicability of formulations devoted to the flexural strengthening of RC members with FRP sheets which are currently reported in both the Italian Guidelines CNR-DT200 R1 [1] and the American ones ACI 440.2R [2].

2. Experimental program

The experimental campaign was carried out at the Laboratory of "Materials and Structural Testing" of the University of Salerno (Italy) and consisted of four-point bending tests performed, in displacement control, on 10 large-scale RC one-way slabs. Of these, 9 specimens were variably strengthened in bending by using SRG or SRP systems, whereas the remaining one, unstrengthened, was used as benchmark.

Detailed information about the geometry of the tested specimens, the strengthening layouts and the test set-up is reported in the following sections.

2.1 RC specimens

Figure 1 shows the geometry and the steel reinforcement of the RC slabs subjected to bending tests. As illustrated, the specimens have a total length of 3700 mm and a 400 x 200 mm^2 rectangular cross-section; the shape of the cross-section, already considered by other authors [5], is representative of shallow beams found in a real structure where the effectiveness of the external SRP reinforcement can be fully exploited.

The longitudinal reinforcement of specimens consists of deformed steel rebars with 10 mm diameter (&). In particular, five (5&10) and two (2&10) rebars made of steel grade "B450C" [19] have been used on the tension and compression side, respectively; on both ends, a concrete cover of 33 mm has been considered.

149 The transverse reinforcement is constituted by steel stirrups with 8 mm diameter and 100 mm spaced.
150 Such reinforcement was designed with the aim to avoid that, in presence of SRG/SRP external
151 strengthening, the shear failure of the beams might occur before the flexural one.
152 Compression and splitting tests were carried out for the mechanical characterization of concrete's
153 properties.
154 The compression tests were performed on eight cubic 150 mm side specimens taken during the slabs'
155 manufacturing and cured under the same environmental conditions. It is highlighted that, although the 10
156 slabs were cast in two different days (in particular, 5 slabs per day), the compression strengths found from
157 the cubic specimens belonging to the two slab's series and tested at about after 4 months' curing, were
158 very similar to each other. Therefore, a unique average value of the cubic compression strength (R_{cm}),
159 equal to 18.24 MPa, can be considered for the two slabs' series, which is associated to a coefficient of
160 variation (CV) of 0.04; the corresponding cylindrical compression strength, f_{cm} (= 0.83 R_{cm}), is equal to
161 15.14 MPa. The motivation for selecting a concrete mix characterized by a medium-low concrete strength
162 lies in the authors' plan of simulating the experimental behaviour of beams belonging to existing
163 structures built in Italy in the '60s and '70s, i.e., when these structures were frequently manufactured
164 using low-performance concrete.
165 The splitting tests were performed on six concrete samples with 95 mm diameter and 95 mm height,
166 which were extracted from three tested slabs; in particular, a couple of concrete cores per considered slab
167 were extracted. The average value of the cylindrical tensile strength (f_{ctm}) estimated from these tests was
168 equal to 2.60 MPa, with a CV value of 0.12; it is highlighted that such an experimental data is
169 significantly higher than the value analytically calculated, for an f_{cm} value of 15.14 MPa, by applying the
170 formulations reported in the Italian Building Code [19].
171 The mechanical properties of steel rebars used as longitudinal and transverse reinforcement were
172 determined from tensile tests performed on small samples. Figure 2 shows the experimental stress-strain
173 behaviours found from these tests (three tests were performed on &10 rebars and five tests on &8
174 specimens), whereas the related mechanical properties are summarized in Table 1. It is first highlighted
175 that all the experimental curves do not exhibit a clearly recognizable yielding condition, and the values of
176 yield strength (f_y) listed in Table 1 are those suggested by the authors for the used rebars. Other
177 information provided in Table 1 is: the ultimate strength (f_t); the hardening ratio (f_t/f_y); the ultimate strain

(ε_t) corresponding to f_t; finally, the last four columns of the table report the average values of the mechanical properties calculated for each set of steel reinforcement ($f_{y,m}$; $f_{t,m}$; $(f_t/f_y)_m$; $\varepsilon_{t,m}$).

2.2 Strengthening materials

Table 2 provides the main information related to the strengthening materials examined in the experimental campaign. In particular, they are unidirectional sheets made of high strength steel cords obtained by twisting steel wires within a micro-fine galvanized coating. Such products, manufactured by Hardwire LLC [20], were applied underneath the beams (via wet lay-up) by using a thixotropic mortar ("SRG system") or a mineral epoxy adhesive ("SRP system"), which are both produced in Italy by "kerakoll S.p.A." [21].

Within the tape, the single cord is typed as "3x2", being made of five filaments: three of these are straight and are wrapped by the other two filaments at a high twist angle. Depending on the number of cords distributed in the tape width, it is possible to define different densities of the reinforcement material. As observed from Table 2, three tape densities (ρ) were examined in the experimental campaign, labelled "GeoSteel G600", "GeoSteel G2000" and "GeoSteel G3300" (in increasing order of the density); it is noted that the number characterizing each label identifies, approximately, the weight of each tape expressed in g/m^2. For the sake of simplicity, the three densities are indicated herein as low ("LD"), medium ("MD") and high ("HD").

In regard to the inorganic matrix used to obtain the SRG strengthening system, an eco-compatible thixotropic mineral mortar (called "Geolite®") has been considered, which is characterized by a very low content of petrochemical polymers, and free from organic fibers. According to the manufacturer [21], the product is an eco-friendly geo-mortar (of alumino-silicate nature) with a crystalline reaction geo-binder base, which is recyclable and characterized by reduced CO_2 emissions and very low volatile organic compounds.

Conversely, the organic matrix employed to yield the SRP strengthening system is a thixotropic epoxy mineral adhesive. According to the manufacturer, it is solvent-free and characterized by very low volatile organic compound emissions, with 46% natural mineral content. Table 2 provides the main mechanical properties of the two considered impregnating matrices as resulting from the technical sheets provided by the supplier [21].

In regard to the characterization of the steel textile used to strengthen the slabs, instead, Table 2 also reports the average values of the relevant mechanical properties obtained from tensile tests performed during a previous experimental campaign on the same steel tapes investigated herein [22].

2.3 Test matrix and specimen preparation

Table 3 reports the text matrix considered for the experimental campaign. In particular, each specimen is identified by a label providing the following information: strengthening system (SRP or SRG), number of sheet layers (1 or 2) and tape density (LD, MD or HD). As an example, the label "SRG-1LD" denotes the slab strengthened by using a single layer of low density steel tape impregnated with inorganic matrix.

The label "US", instead, denotes the unstrengthened specimen, i.e., the "control member" used as comparison term for investigating the performances of the considered strengthening techniques.

As observed from Table 3, three slabs were strengthened with SRP systems and six slabs with SRG ones. In the case of SRP systems, all the three tape densities, applied in a single layer, were investigated. In the case of SRG systems, instead, only low and medium tape densities (applied in a single or double layer) were considered because, unlike the high density, they better allow for the matrix to penetrate through the sheet and create a stronger bond. Also, it is worth highlighting that the particular cord geometry (type "3x2") allows for an improved adhesion and mechanical lock between the grout and the steel cords.

The strengthening with double SRP layer (see specimens "SRG-2LD" and "SRG-2MD" in Table 3), was obtained by overlapping two steel tapes with same length (L_s = 2700 mm), width (b_s = 200 mm) and equivalent thickness (t_{eq} = 0.084 mm and t_{eq} = 0.254 mm for low and medium density, respectively); then, the installation was performed by trying as much as possible to preserve the same cord spacing of the single layer reinforcement. Finally, except for the specimens "SRG-1MD-A" and "SRG-1MD-B", the installation of the strengthening sheet in the laboratory was performed, for practical reasons, by turning upside the tensile end of the slab and working from the above (Fig. 3). However, to check for any reduction of effectiveness when the SRG external reinforcement is installed – as in the real applications – from the bottom, the application of the steel tape on the slabs SRG-1MD-A and SRG-1MD-B was performed after placing these two specimens on a scaffold at a height of about 1.80 m (Fig. 4). Indeed, it is mentioned that the inorganic matrix requires a curing time of about 28 days in order to fully exploit its effectiveness and, throughout this time, local micro-cracks or partial detachments also caused by the

236 weight of the tape, may reduce the efficiency of the reinforcement.

237 Figure 3 shows some relevant steps related to the typical application of the SRG system on the concrete
238 substrate. In particular, the first one is consisted of making the concrete surface rather rough by using a
239 mechanical hammering (Fig. 3a).

240 With the aim to assure an accurate application of the strengthening system, before applying a first layer of
241 mortar, a sort of template, about 5 mm thick, was arranged on the specimen (Fig. 3b). First, the concrete
242 surface was abundantly wetted with water (Fig. 3c) and, then, covered by a first layer of mortar (Fig. 3d).
243 Once applied the tape (Fig. 3e), a second layer of mortar was added (Fig. 2f) and, then, the top layer of
244 the package was wetted again (Fig. 3g). At the completion of these working operations, the strengthened
245 specimen has been wrapped by a nonwoven fabric and by a plastic sheet in order to assure the mortar
246 curing in moist environment (Fig. 3h).

247 The application of the SRP system, instead, did not need some of the key working operations required for
248 the SRG reinforcement, such as: impregnation of the concrete surface with water; use of proper templates
249 and protection of the specimen within the nonwoven fabric and the plastic sheet.

250 For all the strengthened members, each layer of the applied external reinforcement was 2700 mm long
251 and 200 mm wide.

252

253 ## 2.4 Test set-up

254 Specimens were subjected to four-point bending tests by using a 3000 kN MTS hydraulic actuator
255 (stroke: ±75 mm) which was mounted on a proper steel reaction frame, as shown in Figure 5.

256 Tests were carried out in displacement control (displacement rate: 0.02 mm/s), and the corresponding
257 load was measured by both using the load cell integrated in the testing machine (load capacity: 3000 kN
258 and 2500 kN, in compression and tension respectively) and an external 200 kN load cell, which assured a
259 greater accuracy for lower force values.

260 The four-point load was applied through a very stiff steel beam, capable of splitting the total load in two
261 equal forces, 960 mm symmetrically spaced with respect to the slab midspan; the clear length of the
262 simply supported slab was equal to 3400 mm, whereas the shear span measured 1220 mm.

263 Figure 6 shows the position of the two-point load and the arrangement of the measuring equipment used
264 during each test. In particular, the midspan deflection was monitored by using two potentiometers (denoted

with the labels “LV5” and “LV6” in Fig. 6a); in addition to these instruments, two laser sensors were also considered in some tests and placed at the midspan cross-section for a better check of the vertical beam’s displacement. Furthermore, other two couples of potentiometers were arranged at the slab’s center, vertically spaced of about 230 mm between compression and tensile side, in order to measure a mean curvature throughout the loading process. As observed in Figure 6a, the transducers “L01-FS” and “L03-RS” are those placed at beam extrados, whereas “L02-FI” and “L04-RI” are the instruments located just underneath the member.

Finally, a number of strain gauges were arranged for measuring both the compressive strain of concrete at midspan cross-section (gauges “C-01” and “C-02”) and the tensile strain of steel fiber reinforcement at several locations (gauges “F-01” to “F-13”, distributed according to the layout depicted in Fig. 6b).

3. Experimental results and discussion

3.1 Failure mode and load-deflections curves

Table 4 summarizes the main results obtained from the performed tests; in particular:

- F_{max} represents the peak force recorded for each specimen;
- Δ identifies the midspan deflection of each beam corresponding to F_{max};
- I_{Fmax} e I_{Δ} indicate, respectively, the percentage increase of force and the percentage decrease of deflection calculated for each strengthened specimen with respect to the control member (US).

Finally, the last column of Table 4 reports the description of the failure modes observed during the tests which are clearly recognizable from Figures 7-9.

As noted, only the specimens strengthened with a single layer of low density steel tape (i.e., specimens SRP-1LD and SRG-1LD) experienced the tensile rupture of external reinforcement in the constant bending moment region (Fig. 7b,c); this type of failure was observed independently on the nature of the used adhesive (polymeric or inorganic). In particular, in the case of the slab SRP-1LD, the fracture occurred near to the loading point “1” in Figure 6a (see Fig. 7b), whereas in the case of the test SRG-1LD the phenomenon was observed at the beam’s midspan (see Fig. 7c). At the end of the loading process, the two specimens exhibited a rather significant crack pattern in bending which is rather similar to that shown

292 by the unstrengthened member US (see Fig. 7a); such cracks were typically 100 mm spaced, thus
293 covering the same spacing used for transverse steel reinforcement.
294 In all the other performed tests, instead, the failure by SRP/SRG delamination from the concrete substrate
295 was always observed (Figs. 8 and 9). Such failure originally developed in the central region of each
296 member in the form of a longitudinal crack at the concrete-SRP/SRG interface; then, it rapidly propagated
297 towards one of the two slab's ends to finally cause the reinforcement pealing-off.
298 However, it is worth noting that when using the epoxy resin to apply the steel tapes, the delamination
299 clearly involved a rather significant portion of concrete substrate (Figs. 8a and 9a); when employing the
300 inorganic matrix, instead, the collapse of the composite system only partially affected the concrete
301 substrate and, conversely, it more clearly involved the mortar layer, so that an interlaminar delamination
302 in some portions of the beam took place (Figs. 8b,c and 9b).
303 The differences in the delamination mechanism observed for SRP and SRG systems is glaring in Figure 8,
304 where the slab SRP-1MD is compared with the three counterparts strengthened with the SRG
305 reinforcement (SRG-1MD, SRG-1MD-A and SRG-1MD-B). As noted, when employing the inorganic
306 matrix to bond the steel tape with medium density, the removal of a concrete thickness occurred only in
307 some portions of the slabs and, conversely, the adhesive layer kept frequently attached to the beam's
308 intrados. Also, in the case of the slab SRG-1MD, the detachment of the external reinforcement was
309 accompanied by a longitudinal fracture of the steel tape and a significant damage of the constituting cords
310 (Fig. 8b). Such damage was even more evident for the slabs SRG-2LD and SRG-2MD as shown in Figure
311 9b.
312 Disregarding the type of failure mode observed, the experimental results listed in Table 4 allowed for
313 verifying the satisfying behavior exhibited by specimens strengthened with SRG system. As observed,
314 these specimens have experienced strength increases fully comparable with those obtained in the case of
315 SRP strengthened members (for instance, comparisons between specimens SRP-1LD vs. SRG-1LD and
316 SRP-1MD vs SRG-1MD can be made).
317 Good results were also obtained by testing the specimens SRG-1MD-A and SRG-1MD-C for which, as
318 mentioned earlier, the strengthening system was applied by working from the bottom in order to simulate
319 the typical working operations found in the field (Fig. 4). As it can be observed, the two slabs showed a
320 flexural behavior comparable to that exhibited by the member SRG-1MD, which was strengthened

according to more “comfortable” working operations (Fig.3).

The comparisons in terms of load-deflection (F-δ) curves obtained for all the performed tests are shown in Figure 10; in Figure 11, instead, the F-δ experimental behaviors are grouped by the type of strengthening system (SRP or SRG).

It is first highlighted that, the lower initial stiffness characterizing the F-δ curves of both control specimen US and the strengthened ones SRP-1LD and SRG-1MD is due to a pre-cracking accidentally induced in such beams during the transport and assembly operations.

Disregarding the accidental pre-cracking, the slab US showed a first loss of stiffness at a load of about 8.5 kN and another change in the slope of the load-deflection curve at force value of about 37.2 kN; this is of course due to yielding of the tensile steel reinforcement which can be approximately estimated to occur at a midspan deflection of about 24.7 mm. After this threshold, the behaviour of the specimen was characterized by large flexural cracks (Fig. 7a) up to the achievement of the collapse due to concrete crushing in the constant bending moment region.

The F-δ comparison curves show that, disregarding the nature of the matrix, the presence of the strengthening system significantly increases the flexural strength of slabs. From Table 4, it is noted that the percentage strength increases over the control member range from a minimum value of 27%, when using a single layer of low fiber density (“LD”), to a maximum of 106% (more than doubled strength) in the case of SRP system with high density sheet (“HD”). Conversely, as expected, the application of an external strengthening works as an additional tensile reinforcement, thus causing a reduction of the beam’s deflection measured at the achievement of the peak force. Such a reduction generally increases with the amount of the external strengthening and ranges from a minimum of 29% (see the test SRG-1LD in Table 4) to a maximum value of 62% (see the test SRG-1LD-B in Table 4).

In all the cases, at the achievement of the collapse of the steel fiber system, the F-δ curves exhibit a rather abrupt strength decay and, then, the experimental responses start reproducing the typical trend of the unstrengthened member (test US).

Figure 11 better highlights the influence of the steel fiber density and/or the number of layers for a given strengthened system (SRP/SRG). In particular, Figure 11a shows significant increases of strength with the sheet density; indeed, when using the medium density (test SRP-1MD), a strength increase over the test

SRP-1LD equal to 28% was calculated; the percentage goes up to 62% in the case of high density sheet (test SRP-1HD).

From Figure 11b, by focusing on SRG systems, it is possible to both observe the influence of the different sheet density (low and medium) and the number of layers (1 or 2). In particular, in the case of the LD sheet, doubling the number of layers led to 11% strength increase (compare, for instance, SRG-1LD and SRG-2LD). Such an increase is fully comparable with the performance attainable when replacing the double layer of LD sheet with a single layer of MD one (compare, for instance, the specimen SRG-2LD with the three slabs of type "SRG-1MD") although the ratio between the respective sheets' equivalent thicknesses (see Table 2) is about 0.66 (= 2*0.082/0.254). Thus, the obtained result highlights the more efficiency exhibited by SRG systems made of low density steel tapes, since the higher spacing between the steel cords promotes the mortar penetration and create an improved bond.

Finally, in regard to the installation of the medium steel fiber density, the application of two layers (test SRG-2MD) allows for increasing the flexural strength over the use of the single one (tests of "SFRG-1MD" type) of about 29%.

3.2 Local readings of the SRP and SRG strains

As mentioned earlier, the tensile strains in the strengthening sheet were locally monitored during each test by means of 13 strain gauges, arranged on the outer mortar layer of the reinforcement according to the scheme illustrated in Figure 6b.

Figures 12 to 14 show, for some of the tested slabs, two different graphs: in the first one (Figs. 12a to 14a), the experimental SRP/SRG strains were plotted as a function of the total load up to achievement of the maximum force F_{max} (in some cases the strain gauges stopped working before F_{max}); in the second one (Figs. 12b to 14b), instead, the strain profiles along the strengthening sheets (which were 2700 mm long) were plotted at some levels of the acting load, which correspond to percentage values of the peak force. The denomination "central region" identifies the beam's zone subjected to constant bending moment, which was monitored by strain gauges F-04 to F-10 (see Fig. 6b). In particular, the strain gauges F-04/F-05 and F-09/F10 are the couples of sensors placed on the SRG/SRP sheet where the loading points *1* and *2* (in Fig. 6a) were located; as such, these two point data delimiting the "central region" have been

obtained by averaging the readings of strain gauges F-04/F-05 and F-09/F10.

In Figure 12, the experimental diagrams obtained for the slab SRP-1LD are compared with the corresponding plots obtained for the counterpart SRG-1LD. By looking at the strain profiles, it is observed that, as expected, the maximum strains were recorded in the constant bending moment region, but a more regular strain distribution along the reinforcement is observed in the case of the SRP-strengthened slab. Of course, this evidence is also motivated by a non-negligible difficulty experienced in measuring the strain in the SRG systems by strain gauges. Indeed, as mentioned earlier, the sensors were installed on the outer portion of the external reinforcement, where a layer of mortar covers the steel tape; as a result, any micro-cracks induced in the grout during the loading process, eventually developed at strain gauges' location, might have affected the strain reading, and more irregular profiles or lower values might have been recorded. To this purpose, it is observed that, although in terms of flexural strength SRP and SRG systems employing one layer of low density tape gave rise to comparable results (Table 4), the measured SRP strains are generally greater than the SRG ones at any given load level. Differences are also noted from the load-SRP/SRG strain curves; in particular, in the case of the SRP-strengthened slab, trilinear relationships are approximately recognized for the strain measures recorded by gauges F-04 to F-10, with a significant increase of the strain rate at the achievement of the yielding condition (Fig. 12a).

In the case of the SRG strengthened specimen, instead, more complex trends are identified, with reductions of the strain rate recorded by some gauges before the achievement of the yielding condition (Fig. 12b).

As observed, the considerations drawn from Figure 12 can also be extended to the plots shown in Figure 13, related to the SRG/SRP systems employing one layer of medium density steel tape; for the sake of brevity, in this Figure only the strain profiles have been reported for the specimens SRG-1MD-A and SRG-1MD-B.

The graphs shown in Figure 14, referring to the slabs SRP-1HD, SRG-2LD and SRG-2MD, again confirm a more regular trend in the strain profile corresponding to the SRP system; the strain values increase by approaching the null shear region and are approximately constant in that zone, as expected.

Finally, Table 5 summarizes for each test the strain values recorded along the SRP/SRG sheet near the achievement of load peak (F_{max}); the maximum strain measured for each test has been highlighted in italics. Also, the last column of Table 5 reports the average strain values calculated in the portion of the

slab subjected to constant bending moment (i.e., by considering the readings performed by strain gauges F-04 to F-10).

As noted from Table 5, by considering the same steel fiber tape, the strain values recorded for the SRP systems in the constant bending moment region are slightly higher than those measured for the SRG ones. For instance, for the tests SRG-1LD and SRP-1LD the calculated average strain values are equal to 0.95% and 1.34%, respectively; the corresponding maximum strains are 1.49% for the SRG system (strain F-09) and 1.58% for the SRP one (strain F-08), which are both close to the ultimate strain value of the steel tape reported in the technical documents provided by the supplier or experimentally found (see Table 2); this evidence represents a further confirmation of the failure mode experienced during these two tests, i.e, the SRP/SRG fracture in the central region of the specimens.

Similarly, a comparison between the test SRP-1MD and the three tests of type "SRG-1MD" can be made; for the former, the average strain value calculated in the beam's central region is equal to 0.95%, whereas the corresponding value recorded for the SRG system (using the MD tape) is equal to about 0.69. As it can be observed, the maximum strains are rather similar to each other, by approaching the value of 1%.

3.3 Curvatures, mean strains and neutral axes at slabs' midspan

As described in §2.4, two couples of potentiometers were arranged at the midspan of each slab, 230 mm vertically spaced between compression and tensile side, in order to measure a mean curvature throughout the loading process (see transducers "L01-FS"/"L03-RS" and "L02-FI"/"L04-RI" in Figure 6a). By assuming a linear distribution of the strain through the cross-section (i.e, "plane section conservation"), the mean curvature (χ_m) has been evaluated by using the following simplified relationship:

$$\chi_m = \frac{\left|\varepsilon_m^{top}\right| + \left|\varepsilon_m^{bot}\right|}{s_2} = \frac{\left(\left|d_m^{top}\right| + \left|d_m^{bot}\right|\right)/s_1}{s_2} \quad (1)$$

where d_m^{top} and d_m^{bot} represent, respectively, the mean shortenings and elongations measured by the two couples of potentiometers spaced at s_2=230 mm, whereas the corresponding mean strains at compression (ε_m^{top}) and tension (ε_m^{bot}) sides were computed on a measure length of such potentiometers (s_1) equal to 120 mm.

Figure 15 shows the experimental relationships between the bending moment and the curvature at

midspan for some of the tested slabs. As expected, the curves of the strengthened beams can be approximated by trilinear relationships defined through the cracking, yielding and ultimate condition. By focusing on the ultimate stage, characterized by the achievement of the maximum bending moment (M_{max} = $F_{max}/2 \cdot L_s$), it is observed that the corresponding curvature ($\chi_{m,max}$) reduces at increasing the amount of the external reinforcement. It is also noted that, for a given tape density, the maximum curvatures estimated for the SRG systems are higher than the corresponding ones computed for the SRP systems (compare tests SRG-1LD & SRP-1LD; tests SRG-1MD, SRG-1MD-A, SRG-1MD-B & SRP-1LD).

As an alternative to the experimental measure provided by strain gauges, the readings of the potentiometers can be used (by always considering the "plane section conservation") to obtain a further estimate of the compression strain of concrete in compression (ε_c) and of SRP/SRG strain in tension (ε_s). To this purpose, Figure 16 provides, for some representative tests, the comparison between the concrete and SRP/SRG strain estimated by using the abovementioned potentiometers (labeled "SRP/SRG strain" and "concrete strain" in Fig. 16) and the corresponding local strains recorded by averaging the strain gauges C-01/C-02 on the compression side (in some cases C-01 was not working and only the strain gauge C-02 was considered), and F-06/F-07/F-08 on the tensile side (the experimental mean curve is also plotted); such strains have been plotted as a function of the bending moment acting in the "central region" of the slabs. By observing these plots, it is highlighted that, in terms of compression strains, the experimental curves provided by potentiometers "L01-FS"/"L03-RS" generally overlap the measures obtained by strain gauges. In terms of tensile strains, instead, the measures recorded by strain gauges are always lower than that obtained by potentiometers when the slabs are strengthened with SRG systems; this evidence may again validate the consideration on the difficulty of measuring the local SRG strains through strain gauges, being placed on the mortar layer which is significantly affected by the undergoing local damage. Conversely, no specific issues seem to rise in the case of epoxy-bonded steel tapes, as observed for the tests SRP-1LD and SRP-1MD. In particular, for the latter test, a perfect matching is noted between the measure provided by strain gauges and that estimated by potentiometers, whereas for the test SRP-1LD the local strain is even greater than mean one.

A further comparison between the local measure provided by the strain gauges and the mean one recorded by the used potentiometers can be performed in terms of neutral axes evaluated at beam's midspan, as shown for some tests in Figures 17 and 18. In particular, Figures 17a and 18a depict the depth to the

neutral axis (y_c) at some percentage levels of the acting load estimated through the main strains at compression and tensile side of the midspan cross-section provided by potentiometers. In Figures 17b and 18b, instead, the depth to the neutral axis has been plotted by considering, at the tensile side of the cross section, the SRG/SRP mean strain provided by gauges F-06, F-07, F-08; at the compression side, the strain measure deduced from the potentiometers "L01-FS" and "L03-RS" has been considered since, as shown in Figure 16, was quite similar to that provided by gauges C-01 and C-02.

The depths to the neutral axis estimated at the achievement of the peak load (labeled $y_{c,A}$ and $y_{c,B}$ for the neutral axes of Fig. 17a-18a and 17b-18b, respectively) are also compared in Table 5 with the experimental measures ($y_{c,1}$; $y_{c,2}$; $y_{c,3}$) performed at the peak load during the tests, by considering the vertical propagation of three cracks developed approximately at beam midspan (see the picture reported in Table 5); the average value obtained from the three local measures ($y_{c,m}$) is also provided. As expected, the estimate of the neutral axis's depth is sensitive to the type of measure performed at the tensile side of the cross-section. Specifically, by providing a strain averaged on a gauge length s_1 = 120 mm, the measure recorded by the potentiometers is significantly affected by the number of cracks distributed within such length; therefore, the value of d_m^{bot} in Eq. (1) and, consequently, of ε_m^{bot}, increases with the level of cracking catch by these devices. As a result, the depths to the neutral axis listed in Table 5 ($y_{c,A}$), except for one examined case (i.e., test SRP-1LD), are generally lower than the values estimated by using the local strain measures provided by the strain gauges at the tensile side ($y_{c,B}$). Therefore, the choice of using the SRP/SRG strain provided by the strain gauges seems to be preferable, although in same cases may cause an underestimate of the effective strain exhibited in the strengthening systems, mainly for the SRG ones.

4. Analytical predictions at ultimate limit state

As mentioned earlier, no international guidelines are currently available to civil engineers for estimating the flexural strength of RC beams/slabs externally strengthened with either SRP or SRG systems. However, the experimental tests have highlighted that the flexural behaviour of slabs reinforced with SRP composites can be reasonably comparable to that experienced by CFRP-strengthened members; indeed, the performed laboratory tests have highlighted that, when the SRP debonding governed the failure of the slabs (see tests SRP-1MD and SRP-1HD in Figs 8a and 9a), the mechanism occurred similarly to what

known in literature for CFRP systems, i.e., with the removal of a significant concrete's layer underneath the beams.

In the case of SRG systems, instead, the experimental evidence pointed out that the debonding failure of the composite system only partially involves the concrete substrate and, conversely, more clearly affects the grout layer. As a result, unlike the SRP applications, the debonding mechanisms governing the collapse of the SRG systems may not be fully predicted through analytical formulations available for CFRP composite materials, but "ad-hoc" analyses are required for a better understanding of the SRG-to-concrete bond behaviour.

Despite these considerations, the flexural strength of the tested slabs was herein estimated, as a first approximation and disregarding the type of matrix (polymeric or inorganic), according to both the Italian Guidelines CNR-DT200 R1 [1] and the American ones ACI 440.2R [2]; as known, these documents deal with the external strengthening of RC/masonry structures with polymeric matrix-composites employing carbon, glass or aramid fibers and not steel tapes.

In accordance with the considered guidelines, the flexural analysis of SRP/SRG strengthened members was performed by using strain compatibility and force equilibrium methods. The following basic assumptions were considered: 1) plane section before loading remains plane after loading; 2) perfect bond existing between SRG/SRP and concrete, and between steel reinforcement and concrete; 3) tensile strength of concrete is neglected.

For a better modelling of the concrete behaviour in compression, the stress-strain constitutive law proposed by Saenz [23] was considered in place of the simplified equivalent rectangular stress-block proposed by both Guidelines, where the compression strength (f_c) coincides with the experimental mean value f_{cm} = 15.14 MPa, and the ultimate strain ε_{cu} is assumed to be equal to 0.4% (Fig. 19a). An elastic-perfectly plastic law was chosen for simulating the behaviour of the steel rebars in both compression and tension (Fig. 19b), characterized by a yield strength f_y = 460 MPa (which coincides with the experimental mean value $f_{y,m}$ reported in Table 1) and a corresponding strain (ε_y) equal to 0.23%. Finally, the tensile behaviour of the SRP/SRG reinforcement was assumed to be linear-elastic until the failure condition, which is achieved at strength (f_{su}) and strain (ε_{su}) values equal to those reported in Table 2 [22].

By following the indications reported in the two considered Guidelines on the flexural behaviour of RC slabs strengthened with FRP, and extending the basic concepts to the case of SRP/SRG systems, two

519 types of failure can be generally expected, depending on whether the ultimate concrete compressive strain
520 (ε_{cu}) or the maximum SRP/SRG tensile strain (ε_{smax}) is reached; the latter is determined as:

$$\varepsilon_{smax} = min(\varepsilon_{su}; \varepsilon_{sd}) \quad (2)$$

521 where ε_{sd} is the maximum strain due to intermediate debonding failure.

522 According to the American Guide ACI 440.2R [2], the ε_{sd}value can be estimated through the following
523 formulation:

$$\varepsilon_{sd}^{(ACI\ 440)} = 0.41\sqrt{\frac{f_{cm}}{E_s \cdot t_{eq}}} \leq 0.9 \cdot \varepsilon_{su} \quad (3)$$

524 whereas, the Guidelines CNR-DT 200 R1 [1] provide a different relationship:

$$\varepsilon_{sd}^{(DT\ 200)} = \frac{f_{sd}}{E_s} = k_q \cdot \sqrt{\frac{E_s}{t_{eq}} \cdot 2 \cdot k_b \cdot k_{G,2} \cdot \sqrt{f_{cm} \cdot f_{ctm}}} \quad (4)$$

525 In Eq. (4): f_{sd} is the strength corresponding to the debonding failure; k_q is a coefficient accounting for the
526 load distribution (in this case, k_q =1); $k_{G,2}$ (= 0.32) is a corrective factor calibrated on experimental
527 results; k_b is a geometrical corrective factor depending on the ratio between the SRP/SRG external
528 reinforcement width (b_s) and the concrete one (b) (in this case, b_s/b = 0.5), which is calculated by means
529 of the following relationship:

$$k_b = \sqrt{\frac{2 - b_s/b}{1 + b_s/b}} \geq 1 \quad (5)$$

530 It is highlighted that Eq. (4) has been written herein without any reduction factor required for design
531 purposes. Regarding the mean value of the concrete tensile strength (f_{ctm}), instead, the following
532 formulation reported in the Italian Building Code (19) has been selected, by considering an increase of f_{ctm}
533 by 1.2 factor (f_{cfm} = 1.2 f_{ctm}) to account for the tensile strength of concrete in bending:

$$f_{cfm} = 1.2 \cdot f_{ctm} = 1.2 \cdot 0.30 \cdot (f_{ck})^{2/3} = 1.2 \cdot 0.30 \cdot (f_{cm} - 8)^{2/3} \quad (6)$$

534 The analytical results obtained by applying the formulations suggested by DT200 [1] and ACI 440 [2] to
535 all the performed tests are reported in Tables 7 and 8, respectively. In particular, the following
536 information at ultimate limit state is reported in each Table:

537 ✓ the maximum SRP/SRG tensile strain ε_{smax} estimated for each test which always coincides with
538 the debonding one ($\varepsilon_{smax} = \varepsilon_{sd}$);

- ✓ the strain values of the SRP/SRG sheet (ε_s), the steel reinforcement both in tension (ε_f) and compression (ε'_f) and concrete (ε_c);
- ✓ the stress values of the SRP/SRG sheet (σ_s), the steel reinforcement both in tension (σ_f) and compression (σ'_f);
- ✓ the depth to the neutral axis (y_c);
- ✓ the values of the maximum bending moment (M_{max}) and total force (F_{max}) estimated for each test which are compared with the corresponding experimental results.

Finally, the last column of each Table reports the computed mean absolute percentage error (E_{rr}) between the experimental and the theoretical value of the force F_{max}.

By comparing the theoretical results reported in Tables 7 and 8 it is highlighted that, disregarding the type of formulation applied for estimating the ε_{sd} value (Eq. 3 or 4), the SRP/SRG debonding mechanism always governed the failure of all the strengthened beams, with maximum strains rather similar to those experimentally measured by strain gauges in the constant bending moment region (see Table 5); also, the two different relationships give rise to similar values of ε_{sd}, with slightly higher strains estimated by using Eq. (4).

By looking at the computed errors, it can be noted that the application of Eq. (4) suggested by DT200 generally allows for providing a slightly better prediction of the beam's flexural strength. Disregarding the given guidelines, the analytical results generally well match the experimental ones in the case of slabs strengthened with one layer of low and medium density steel tape, whereas provide conservative predictions in the remaining cases; the major discrepancies are noted at increasing the equivalent thickness of the external reinforcement, as in the cases of slabs SRP-1HD and SRG-2MD. Therefore, the considerations drawn from the few experimental-theoretical comparisons, although do not allow for an exhaustive analysis on the performance of the considered relationships, highlight the need to develop a more accurate modelling of the concrete-SRP/SRG interface capable of better predicting the debonding mechanism and, so, the flexural strength of the strengthened slabs. In particular, by focusing on Eq. (4), it seems that, in the case of the SRP systems, for which the debonding mechanism is comparable to that occurring for CFRP systems, a better prediction may be easily obtained by changing the value of the

parameter $k_{G,2}$, being a corrective factor calibrated on experimental results of FRP strengthened slabs. Conversely, in the case of the SRG systems, a specific revision of Eq. (4) is required, which better accounts for the differences observed in the delamination phenomenon exhibited when using the inorganic matrix to bond the steel tapes.

5. Some considerations about SRP systems

In this section, some preliminary considerations related to either the shear (τ) and normal stresses (σ_n) developed at the concrete/SRP interface or the longitudinal stress acting in the external reinforcement (σ_s) are drawn. To this purpose, some analytical relationships found from the literature [24] or proposed by the mentioned DT200 [1] and ACI 440 [2] documents – although suitable for FRP-strengthened RC members – were taken into account and applied to SRP reinforcements; then, the obtained results were compared with the experimental ones.

It is worth highlighting that the discussion presented herein is restricted only to SRP systems due to the comparable debonding mechanisms activated for SRP and FRP strengthened members, as already mentioned in §4. Conversely, a specific analysis is deserved to SRG systems, for which the observed debonding mechanisms, also highlighted in bond tests published in [25], require an accurate study of the concrete-SRG interface.

In particular, the study presented herein was devoted to investigate if the intermediate debonding experienced during the tests can be accurately predicted by using theoretical formulations. As known, the most important types of debonding failure recognizable in the case of RC members flexurally strengthened with FRP (and so, with SRP) are: *a)* the plate end debonding (namely, "Mode 1" failure) and, *b)* the intermediate debonding by flexural cracks (namely, "Mode 2" failure) or by diagonal shear cracks (namely, "Mode 3" failure) [1].

Specifically, the failure Mode 1, which is activated at or near a plate end, is generally due to a combination of high interfacial shear stresses τ (generally acting on a length of approximately 100 – 200 mm from the sheet end) and tensile stresses perpendicular to the interface between external reinforcement and concrete (i.e., the normal stresses, σ_n); the latter ones may significantly arise due to the high stiffness of the external reinforcement, thus reducing the allowable interfacial shear stresses, as shown by the

delamination circle tangential to the Mohr-Coulomb criterion failure [24]. This delamination circle is defined through a relationship between the maximum shear stress τ_{lmax} and the maximum normal (peeling) stress σ_{nmax}, which in turn can be expressed as a function of the concrete compressive strength f_{cm} and the concrete tensile strength f_{ctm} as follows:

$$\tau_{lmax}^2 = F \cdot f_{cm} \cdot f_{ctm} - F \cdot (f_{cm} - f_{ctm}) \cdot \sigma_{nmax} - F \cdot \sigma_{nmax}^2 \quad (7)$$

where:

$$F = \frac{f_{cm} \cdot f_{ctm}}{(f_{cm} + f_{ctm})^2} \quad (8)$$

and σ_{nmax} is the maximum peeling stress obtained at the sheet end, i.e., by plugging x=0 in Eq. (9), which is derived from a linear –elastic analysis [24]:

$$\sigma_n(x) \approx \frac{K_n \cdot M_0}{2 \cdot \beta^2 \cdot E_c \cdot I_c} \cdot e^{-\beta x}[cos(\beta x) - sin(\beta x)] \quad (9)$$

In Eq. (9):

- $M_0 = F/2\ L_0$ is the bending moment acting at the laminate end (x = 0) which, in the examined cases, is located at a distance l_0 = 350 mm from the beam support (see Fig. 6a);
- E_c is the modulus of elasticity of the concrete which can be estimated according to the following formulation reported in the Italian Building Code (19):

$$E_c = 22000 \cdot \left(\frac{f_{cm}}{10}\right)^{0.3} \quad \text{(MPa)} \quad (10)$$

- I_c is the second moment of inertia of the concrete;
- β is defined by:

$$\beta = \sqrt[4]{\frac{K_n \cdot b_s}{4 \cdot E_s \cdot I_s}} = \sqrt[4]{\frac{E_a/t_a \cdot b_s}{4 \cdot E_s \cdot I_s}} \quad (11)$$

where E_a and t_a denote the elastic modulus and the thickness of the adhesive (epoxy) layer, and I_s represents the second moment of inertia of the SRP sheet.

As observed from Eq. (7), the value of τ_{lmax} significantly reduces at increasing the value of $\sigma_{nmax,}$ whereas attains the maximum threshold when the acting peeling stress is equal to zero, i.e. when $\tau_{lmax} = \tau_{lm}$, corresponding to the "pure" shear condition. In this case:

$$\tau_{lmax} = \tau_{lm} = \frac{f_{cm} \cdot f_{ctm}}{f_{cm} + f_{ctm}} \quad (12)$$

Figure 20 shows the behavior of the peeling stress function obtained by applying Eq. (9) to the three examined cases, i.e.: test SRP-1LD, SRP-1MD and SRP-1HD. In plotting this function, a value of E_a = 5300 MPa (see Table 2) has been assumed, whereas two different thicknesses of the adhesive layer have been considered (0.5 and 1.5 mm); furthermore, the values of F/2 = F_{max}/2, experimentally obtained for each test, have been plugged in Eq. (9) (see F_{max} in Table 4).

As observed from Figure 20, independently on the value of t_a, the σ_n function tends very quickly to zero and achieves very low values even for x = 0 (i.e. at the laminate end), where $\sigma_n = \sigma_{nmax}$ is equal to 0.0002 MPa, 0.0013 MPa, 0.0031 MPa for specimens SRP-1LD, SRP-1MD and SRP-1HD, respectively. The very low value of σ_{nmax} (≈ 0 MPa) implies that the maximum shear stress occurring at a plate end debonding, equal to about 1.035 MPa for all the three examined cases (from Eq. 7), approximately coincides with that obtainable by considering Eq. (12), i.e., in the case of "pure" shear condition.

The estimated value of τ_{lmax} can be then compared with the experimental data of the interfacial SRP-concrete shear stresses calculated by using the strain gauges' readings available in the "shear span" (see strain gauges F-01 to F-05 and F-09 to F-13 in Fig. 6b). Such experimental mean values, shown in Figures 21a, 22a and 23a for the three considered cases, have been obtained at some percentage levels of F_{max}, according to the following relationship:

$$\tau = \frac{(\varepsilon_2 - \varepsilon_1) \cdot E_s \cdot t_{eq}}{x_2 - x_1} \quad (13)$$

where ε_1 and ε_2 identify the strain measures recorded by two adjacent strain gauges, spaced at (x_2-x_1).

As noted, in the case of the specimen SRP-1LD (Fig. 21a), the estimated value of τ_{lmax} ≈ 1.035 MPa is significantly higher than the experimental data plotted by using Eq. (13); this observation implies that, in such test, the debonding mechanism did not affect the collapse of the slab, as confirmed by the experimental evidence (fracture of the SRP system at the slab midspan was experienced for this test).

Conversely, by approaching the bending moment region, the value of τ_{lmax} is overcome in the case of the specimen SRP-1HD (Fig. 22a) and almost matched in the test SRP-1MD (Fig. 23a); therefore, the result confirms that the debonding failure took place in these two experimental tests.

Another consideration about the types of SRP debonding failure observed during the tests can also be performed by estimating the debonding strengths achievable in plate end debonding failure (Mode 1) and intermediate debonding by flexural cracks failure (Mode 2); to this purpose, the predictive relationships suggested by DT200 [1] and ACI 440 [2] documents have been considered.

In particular, according to DT200, the debonding strength in Mode 1 is given by:

$$f_{sd,mode\ 1}^{(DT200)} = \sqrt{\frac{2 \cdot E_s \cdot \Gamma_{Fd}}{t_{eq}}} \tag{14}$$

where Γ_{Fd} is the specific fracture energy estimated through the following relationship:

$$\Gamma_{Fd} = k_b \cdot k_G \cdot \sqrt{f_{cm} \cdot f_{ctm}} \tag{15}$$

where k_G (= 0.077) is a corrective factor calibrated on experimental results.

The debonding strength due to flexural crack (Mode 2), instead, is obtained by multiplying Eq. (4) by the elastic modulus E_s:

$$f_{sd,mode\ 2}^{(DT200)} = k_q \cdot \sqrt{\frac{E_s}{t_{eq}} \cdot 2 \cdot k_b \cdot k_{G,2} \cdot \sqrt{f_{cm} \cdot f_{ctm}}} \tag{16}$$

Similarly, the formulation provided by ACI 440 to estimate the debonding strength in Mode 2 failure derives from Eq. (3):

$$f_{sd,mode\ 2}^{(ACI\ 440)} = 0.41 \sqrt{\frac{E_s \cdot f_{cm}}{t_{eq}}} \tag{17}$$

Figures 21b, 22b and 22b show, for the tests under consideration, the distribution of the longitudinal tensile stress in the SRP reinforcement experimentally computed at some percentage levels of the force F_{max}; such values derive from the strain distributions illustrated in Figures 12-14 and multiplying them by the elastic modulus of the steel tape E_s. Also, the values of the debonding strength in both Mode 1 and 2, estimated according the mentioned Eqs. (14), (16) and (17), are shown in these plots and compared with the experimental data.

As observed in Figure 21b, related to the test SRP-1LD, the estimated value of $f_{sd,mode\ 1}^{(DT200)}$ is significantly higher than the maximum longitudinal stresses measured toward the sheet end, thus confirming that the failure of the slab was not governed by a such debonding mechanism. Conversely, the estimated values of $f_{sd,mode\ 2}^{(DT200)}$ and $f_{sd,mode\ 2}^{(ACI\ 440)}$ are overcome by the experimental stress values but, as

mentioned earlier, in this test the fracture of the SRP system at the slab midspan was experienced.

By observing the plot in Figure 22b and 22c, related to the tests SRP-1MD and SRP-1HD, respectively, it is noted that the values of $f_{sd,mode\,1}^{(DT200)}$ are again lower than the experimental stress data measured at the sheet ends; conversely, the values of $f_{sd,mode\,2}^{(DT200)}$ and $f_{sd,mode\,2}^{(ACI\,440)}$ are significantly overcome by approaching the constant bending moment regions, meaning that intermediate debonding took place for these specimens, as experimentally observed.

6. Conclusions

In this paper, the experimental results of four-point bending tests performed on RC one-way slabs strengthened with SRP/SRG systems have been presented and discussed.

In addition to the nature of the used adhesive (polymeric or cementitious), the main study parameters were the number of layers (one or two), the steel tape density (low, medium or high) and, in the case of the SRG system, the way of strengthening installation (from the top or the bottom).

The performed tests have shown that, disregarding the type of adhesive, the slabs strengthened with one layer of low density tape (specimens SRG-1LD and SRP-1LD) have both experienced the fracture of the sheet in the constant bending moment region. In all the other cases, instead, an SRP/SRG delamination failure was always observed. However, in regard to SRG-strengthened slabs, the collapse of the strengthening system has significantly involved the mortar layer, whereas only a limited removal of concrete substrate, concentrated in a few zones of the beam length, was experienced as otherwise observed in the case of SRP systems.

Regardless of the observed failure mode, test results have allowed for verifying the good performance exhibited by RC slabs strengthened with SRG systems which have shown strength increases comparable to those obtained from companion specimens strengthened with SRP. The efficiency of the SRG system was even more evident when using the low density (LD) tape, both in single or double layer; in particular, the slab strengthened with two SRG layers showed an increase of strength fully comparable to that provided by specimens strengthened with one layer of medium density (MD) tape, characterized by a thickness of 1.5 times over that obtained with two LD layers.

By looking at the strain profiles plotted by using the strain gauges' readings, a more regular strain

686 distribution along the external reinforcement was observed in the case of the SRP-strengthened slabs,
687 with values that are generally greater than those measured in the SRG companion specimens. This
688 evidence was also motivated by the unquestionable difficulty in recording the strain in the SRG systems
689 through strain gauges, since any micro-cracks induced in the grout during the loading process of the slabs,
690 eventually developed at strain gauges' location, might have affected the strain reading, and more irregular
691 profiles or lower values might have been recorded.
692 Finally, preliminary analytical studies were performed for verifying, as a first approximation, the
693 possibility of extending the applicability of formulations currently reported in both the Italian Guidelines
694 CNR-DT200 R1 and the American Guide ACI 440.2R for the flexural strengthening of RC members with
695 FRP sheets; the main difference existing between the two documents lies in the formulation adopted for
696 estimating the maximum strain of the external reinforcement due to intermediate debonding failure. By
697 focusing on SRP systems only, some considerations related to either the shear and normal stresses
698 developed at the concrete/SRP interface or the longitudinal stress acting in the external reinforcement
699 were also drawn.
700 The results of the performed study have shown a slightly better prediction of the beam's flexural strength
701 obtained by using the formulation suggested by DT200. Disregarding the used guidelines, the analytical
702 results generally well match the experimental ones in the case of slabs strengthened with one layer of low
703 and medium density steel tape, whereas provide conservative predictions in the remaining cases; the
704 major discrepancies are noted at increasing the equivalent thickness of the external reinforcement.
705 However, regardless of the greater or lesser accuracy of the obtained results, the preliminary analytical
706 study has highlighted the need to develop a refined modelling of the concrete-SRP/SRG interface
707 behaviour, capable of better predicting the debonding mechanism and, so, the flexural strength of the
708 strengthened slabs. This consideration is even more relevant in the case of the SRG systems due to the
709 different delamination phenomenon exhibited when using the inorganic matrix to bond the steel tape to
710 the concrete surface.
711

712 ## Acknowledgements

713 The Authors would like to thank Kerakoll S.p.A. (Sassuolo, Italy) for the technical and financial support
714 to the experimental program.

715 The Authors also gratefully acknowledge the financial support provided by “ReLUIS” for the research
716 program funded by the Department of Civil Protection – Executive Project 2015.
717 Special thanks are extended to Engs. Francesco Perri and Bruno Nunziata for the assistance in the
718 laboratory work.
719

References

[1] CNR-DT200 R1. Guide for the Design and Construction of Externally Bonded FRP Systems For Strengthening Existing Structures (Materials, RC and PC Structures, masonry structures). CNR, National Research Council 2013, Rome, Italy.

[2] ACI 440.2R. Guide for the Design and Construction of Externally Bonded FRP Systems for Strengthening Concrete Structures. ACI, American Concrete Institute, 2008, Farmington Hills, MI (USA).

[3] Wobbe E, Silva P, Barton BL, Dharani LR, Birman V, Nanni A, Alkhrdaji T, Thomas J, Tunis T. Flexural Capacity of R/C Beams Externally Bonded with SRP and SRG". In: *Proc. of Society for the Advancement of Material and Process Engineering Symp.* (2004), Long Beach, Ca, Usa: 20-27.

[4] Prota A, Manfredi G, Nanni, Cosenza E, Pecce M. Flexural Strengthening of R/C Beams Using Emerging Materials: Ultimate Behavior". In: *Proc. of Cice 2004*, Adelaide, Australia: 163-170.

[5] Prota A, Tan KY, Nanni A, Pecce M, Manfredi G. Performance of shallow R/C beams with externally bonded steel-reinforced polymer. *ACI Structural J.* 2006; 103(2): 163-170.

[6] Kim JY, Fam A, Kong A, El-Hacha R. Flexural Strengthening of RC Beams using steel reinforced polymer (SRP) Composites. In: *Proc. of the 7th Int. Symp. FRP Reinforcement for Concrete Structures*, ACI SP-230 2005, 1, Paper #93: 1647-1664.

[7] W. Figeys, L. Schueremans, K. Brosens, D. Van Gemert, "Strengthening of Concrete Structures Using Steel Wire Reinforced Polymer". *Proc. of the 7th Int. Symp. Frp Reinforcement For Concrete Structures, ACI SP-230* 2005, 1, Paper #43: 743-762.

[8] Huang X, Birman V, Nanni A, Tunis G. Properties and potential for application of steel reinforced polymer and steel reinforced grout composites. *Composites: Part B* 2005; 36: 73–82.

[9] Balsamo A, Nardone F, Iovinella I, Ceroni F, Pecce M. Flexural strengthening of concrete beams with EB-FRP, SRP and SRCM: experimental investigation. *Composites: Part B* 2013; 46: 91–101.

[10] Hawileh R, Abdalla J, Nawaz W, Alzeer A, Muwafi R, Faridi A. Strengthening reinforced concrete beams in flexure using hardwire steel fiber sheets. In: *Proc. of Cice 2014*, Vancouver, Canada, August 20-22, 22 pp.

[11] Pecce M, Ceroni F, Prota A, Manfredi G. Response prediction of R/C beams externally bonded with steel reinforced polymers". *J. of Composites for construction* 2006; 103 (2): 195-203.

[12] Barton B, Wobbe E, Dharani LR, Silva P, Birman V, Nanni A, Alkhrdaji T, Thomas J, Tunise G.

749 Characterization of reinforced concrete beams strengthened by steel reinforced polymer and grout (SRP
750 and SRG) composites. *Materials Science and Engineering: A* 2005; 412 (1-2): 129-136.
751 [13] Ceroni F, Pecce M. Cracking behaviour of RC beams externally strengthened with emerging
752 materials. *Construction and Building Materials* 2007; 21: 736–745.
753 [14] Casadei P, Nanni A, Alkhrdaji T, Thomas J. Performance of double-t prestressed concrete beams
754 strengthened with steel reinforced polymer. *Advances in Structural Engineering* 2005; 8(4): 427-442.
755 [15] Lopez A, Galati N, Alkhrdaji T, Nanni A. Strengthening of a reinforced concrete bridge with
756 externally bonded steel reinforced polymer (SRP). *Composites: Part B* 2007; 38: 429–436.
757 [16] ACI 440. Guide for the Design and Construction of Externally Bonded FRP Systems for
758 Strengthening Concrete Structures. ACI, American Concrete Institute, 2002, Farmington Hills, MI
759 (USA).
760 [17] Matana M, Nanni A, Dharani L, Silva P, Tunis G. Bond Performance of Steel Reinforced Polymer
761 and Steel Reinforced Grout. In: *Proc. of Bbfs 2005,* Hong Kong, China, December 7-9.
762 [18] Mitolidis GJ, Salonikios TN, Kappos AJ. Mechanical and bond characteristics of SRP and CFRP
763 reinforcement – A comparative research. *The Open Construction and Building Technology J.* 2008; 2: 207-
764 216.
765 [19] Decreto Ministeriale 14 gennaio 2008. Norme Tecniche per le Costruzioni (NTC), G.U. n.29 del 4
766 febbraio 2008. [in italian].
767 [20] Hardwire LLC - web site: www.hardwirellc.com *(accessed date: Jan 2015)*
768 [21] Kerakoll S.p.A. - web site: www.kerakoll.com *(accessed date: Jan 2015)*
769 [22] Faella C, Napoli A, Perri F, Realfonzo R. Confinamento del calcestruzzo mediante impiego di tessuti
770 in fibra d'acciaio. In: *Proc. of "Giornate AICAP 2014",* Bergamo, Italy, May 22-24, 8pp. [in italian].
771 [23] Saenz LP. Equation for the stress-strain curve of concrete in uniaxial and biaxial compression of
772 concrete. *ACI Journal* 1965; 61(9): 1229-1235.
773 [24] Brosens K. Anchorage of externally bonded steel plates and CFRP laminates for the strengthening of
774 concrete elements. *PhD thesis,* Katholieke Universiteit Leuven, 2001, 275 pp.
775 [25] Napoli A, Realfonzo R. Sistemi SFRP e SFRG per il rinforzo di elementi in calcestruzzo: risultati di
776 test di delaminazione. In: *Proc. of "XX Congresso CTE*", Milano, 2014, November 6-8: 21-30 [in Italian].
777

Figure captions

Figure 1 – Geometry and the steel reinforcement configuration of the RC slabs.

Figure 2 – Stress-strain laws characterizing the behaviour of the used longitudinal and transverse steel reinforcement.

Figure 3 – Typical working operations required for the installation of the SRG strengthening system.

Figure 4 – Installation of the strengthening system simulating the real applications: working procedure from the bottom.

Figure 5 – Test set-up.

Figure 6 – Instrumentation.

Figure 7 – Failure modes: specimens US (a); SRP-1LD (b); SRG-1LD (c).

Figure 8 – Failure modes: specimens SRP-1MD (a); SRG-1MD (b); SRG-1MD-A & SRG-1MD-B (c).

Figure 9 – Failure modes: specimens SRP-1HD (a); SRG-2LD & SRG-2MD (b).

Figure 10 – Load - midspan deflection curves of all test specimens.

Figure 11 – Load - midspan deflection curves for: SRP systems (a); SRG systems (b).

Figure 12 – Local readings of the SRP/SRG strains: specimens SRP-1LD, SRG-1LD.

Figure 13 – Local readings of the SRP/SRG strains: specimens SRP-1MD, SRG-1MD, SRG-1MD-A & SRG-1MD-B.

Figure 14 – Local readings of the SRP/SRG strains: specimens SRP-1HD, SRG-2LD & SRG-2MD.

Figure 15 – Bending moment-curvature experimental curves for some tested beams.

Figure 16 – Comparison between the local strains measured by strain gauges and the means ones obtained by potentiometers.

Figure 17 – Slabs strengthened with a single layer of low density steel tape: depth to the neutral axis at some load levels obtained by using (a) potentiometers' measures at both compression and tension side; (b) potentiometers' measures at compression side and strain gauges' readings at tension one.

Figure 18 – Slabs strengthened with a single layer of medium density steel tape: depth to the neutral axis at some load levels obtained by using (a) potentiometers' measures at both compression and tension side; (b) potentiometers' measures at compression side and strain gauges' readings at tension one.

Figure 19 – Constitutive laws assumed for: concrete in compression (a); steel reinforcement in

tension/compression (b); (c) SRG/SRP system in tension.

Figure 20 – Interfacial normal stress along the SRP sheets: tests SRP-1LD, SRP-1MD, SRP-1HD.

Figure 21 – Interfacial shear (a) and longitudinal stress (b) along the SRP sheet: test SRP-1LD.

Figure 22 – Interfacial shear (a) and longitudinal stress (b) along the SRP sheet: test SRP-1MD.

Figure 23 – Interfacial shear (a) and longitudinal stress (b) along the SRP sheet: test SRP-1HD.

Table

Click here to download Table: Tables_June 4_2015.docx

Table 1. Steel rebars' properties

Steel Reinforcement	Diameter [mm]	Test N.	f_y [MPa]	f_t [MPa)	f_t/f_y [-]	ϵ_t [%]	$f_{y,m}$ [MPa]	$f_{t,m}$ [MPa]	$(f_t/f_y)_m$ [-]	$\epsilon_{t,m}$ [%]
Longitudinal	10	1	460.1	657.2	1.43	7.16	460	655	1.42	7.72
		2	462.7	655.7	1.42	6.97				
		3	458.9	652.2	1.42	9.03				
Transverse	8	1	521.3	685.5	1.31	5.42	524	690	1.32	7.10
		2	521.5	688.6	1.32	7.38				
		3	524.5	682.7	1.30	8.41				
		4	523.5	709.8	1.36	7.68				
		5	527.0	682.1	1.29	6.62				

Table 2. Typology and mechanical properties of the used strengthening materials

STEEL TAPE		
Effective area of one cord "3x2"	A_{cord} = 0.538 mm^2	
Ultimate tensile strength*	f_{su} > 2800 MPa	f_{su} = 3302 MPa
Modulus of elasticity*	E_s > 190000 MPa	E_s = 206600 MPa
Ultimate tensile strain	ε_{su} > 1.50%	ε_{su} = 1.80%
**Properties related to the dry sheet*	*(Data provided by supplier)*	*(Data determined experimentally [22])*

Low density (LD)	***Medium density (MD)***	***High density (HD)***
		
GEOSTEEL G600	**GEOSTEEL G2000**	**GEOSTEEL G3300**
N. cord/mm, ρ: 0.157	N. cord/mm, ρ: 0.472	N. cord/mm, ρ: 0.709
Weigth, w: 0.67 kg/m^2	Weigth, w: 2.00 kg/m^2	Weigth, w: 3.30 kg/m^2
Equivalent thickness $t_{eq} = A_{cord} \cdot \rho$: 0.084 mm	Equivalent thickness $t_{eq} = A_{cord} \cdot \rho$: 0.254 mm	Equivalent thickness $t_{eq} = A_{cord} \cdot \rho$: 0.381 mm

MATRIX (mechanical properties at 28 days of curing)			
GEOLITE® – Thixotropic mineral mortar		***GEOLITE® GEL – Epoxy mineral adhesive***	
Compressive strength	> 55 MPa	Tensile strength	> 14 MPa
Tensile strength in bending	> 10 MPa	Shear strength	> 20 MPa
Modulus of elasticity in compression	= 25000 MPa	Modulus of elasticity in compression	> 5300 MPa

Table 3. Test matrix

Test #	Test Identification	Type of matrix	N. of layers	Tape density
1	US	–	–	–
2	SRP-1LD	polymeric	1	Low
3	SRP-1MD		1	Medium
4	SRP-1HD		1	High
5	SRG-1LD	grout	1	Low
6	SRG-2LD		2	Low
7	SRG-1MD		1	Medium
8	SRG-1MD-A		1	Medium
9	SRG-1MD-B		1	Medium
10	SRG-2MD		2	Medium

Table 4. Test results and failure modes

Test	F_{max} [kN]	Δ [mm]	I_{Fmax} [%]	I_{Δ} [%]	Failure mode
US	45.23	137.61	–	–	Concrete failure in compression
SRP-1LD	57.30	86.03	26.70	-37.49	Fracture of the SRP system at the slab midspan
SRP-1MD	73.15	72.56	61.75	-47.27	SRP delamination
SRP-1HD	93.10	69.96	105.86	-49.16	SRP delamination
SRG-1LD	61.85	97.16	36.76	-29.39	Fracture of the SRG system at the slab midspan
SRG-2LD	68.70	76.28	51.91	-44.57	Delamination of the SRG system
SRG-1MD	69.55	57.10	53.79	-58.51	Delamination of the SRG system
SRG-1MD-A	70.25	53.49	55.33	-61.13	Delamination of the SRG system
SRG-1MD-B	64.28	51.79	42.12	-62.37	Delamination of the SRG system
SRG-2MD	87.58	54.65	93.64	-60.29	Delamination of the SRG system

Table 5. Strains measured in the strengthening system at the achievement peak load

Test	F_{max} [kN]	F-01 [%]	F-02 [%]	F-03 [%]	F-04 [%]	F-05 [%]	F-06 [%]	F-07 [%]	F-08 [%]	F-09 [%]	F-10 [%]	F-11 [%]	F-12 [%]	F-13 [%]	$\varepsilon_{s,m}^{*}$ [%]
SRP-1LD	57.30	0.117	0.215	0.337	1.153	-	-	-	***1.582***	1.374	0.268	0.484	0.242	-	1.344
SRP-1MD	73.15	0.152	0.350	0.766	0.908	1.052	***1.123***	0.993	0.938	0.706	0.944	0.706	0.287	0.040	0.952
SRP-1HD	93.10	0.074	0.397	0.529	0.909	0.918	***0.969***	0.947	0.797	0.717	0.929	0.608	0.435	0.177	0.884
SRG-1LD	61.85	0.051	0.209	0.436	0.578	1.055	1.093	0.692	0.781	***1.486***	-	0.576	0.386	0.105	0.947
SRG-2LD	68.70	0.131	0.269	0.679	0.834	0.505	0.808	***1.073***	1.015	1.022	1.037	0.642	0.254	-	0.899
SRG-1MD	69.55	-	0.178	0.448	0.667	0.667	0.728	0.765	0.455	***0.799***	0.663	1.287	0.221	0.131	0.678
SRG-1MD-A	70.25	0.198	0.212	0.385	0.626	0.620	0.635	***0.846***	0.693	-	0.728	0.535	0.257	0.066	0.691
SRG-1MD-B	64.28	0.061	0.194	0.462	0.559	***1.458***	0.623	0.559	0.605	0.559	0.522	0.584	0.217	0.049	0.698
SRG-2MD	87.58	0.239	0.269	0.478	***0.746***	0.612	0.563	0.714	0.610	0.523	-	-	-	-	0.628

** Value obtained by averaging the strain readings provided by strain gauges F-04 to F-10*

Table 6. Measured and estimated values of the neutral axis's depth at the peak load

	Measured					*Estimated*	
Test	$y_{c,1}$ [mm]	$y_{c,2}$ [mm]	$y_{c,3}$ [mm]	*$y_{c,m}$ [mm]*	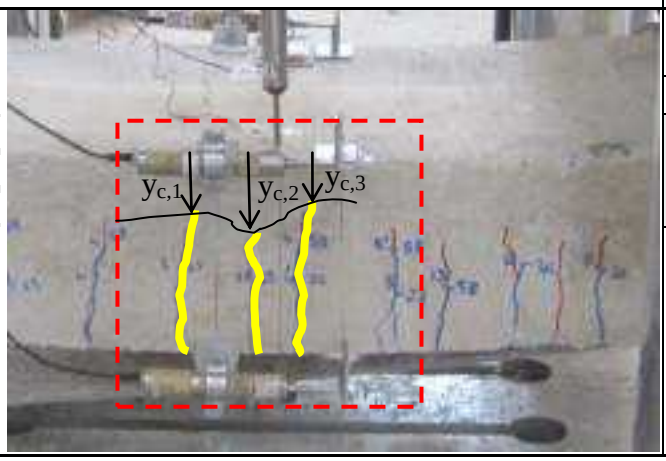	$y_{c,A}$ [mm]	$y_{c,B}$ [mm]
US	24.1	51.8	46.5	*40.8*		41.9	–
SRP-1LD	46.5	42.8	46.5	*45.3*		54.1	38.6
SRP-1MD	54.3	46.4	61.5	*54.1*		52.7	53.1
SRP-1HD	87.3	43.7	52.4	*61.1*		–	–
SRG-1LD	50.3	54.1	50.3	*51.5*		23.5	44.6
SRG-2LD	44.8	72.8	44.8	*54.2*		–	–
SRG-1MD	47.7	56.7	66.2	*56.9*		36.4	61.6
SRG-1MD-A	57.1	64.3	50.0	*57.1*		17.4	30.7
SRG-1MD-B	53.5	66.8	57.9	*59.4*		27.2	52.3
SRG-2MD	60.2	62.1	56.3	*59.6*		–	–

Table 7. Theoretical predictions according to CNR-DT 200 R1 [1]

										theoretical		*experimental*		
Test	$\varepsilon_{smax} = \varepsilon_{sd}$ [%]	ε_s [%]	ε_f [%]	ε'_f [%]	ε_c [%]	σ_s [MPa]	σ_f [MPa]	σ'_f [MPa]	y_c [MPa]	M_{max} [kN m]	F_{max} [kN]	M_{max} [kN m]	F_{max} [kN]	E_{rr} (%)
US	–	–	–	–	–	–	460	77	33.1	27.82	45.61	27.59	45.23	0.83
SRP-1LD	1.31	1.31	1.07	0.08	0.32	2531	460	160	39.5	35.07	57.49	34.95	57.30	0.33
SRP-1MD	0.75	0.75	0.61	0.09	0.24	1456	460	184	48.0	40.16	65.84	44.62	73.15	10.00
SRP-1HD	0.62	0.62	0.49	0.09	0.22	1189	460	194	52.5	42.75	70.09	56.79	93.10	24.72
SRG-1LD	1.31	1.31	1.07	0.08	0.32	2531	460	160	39.5	35.07	57.49	37.73	61.85	7.05
SRG-2LD	0.93	0.93	0.75	0.08	0.26	1790	460	174	44.2	37.96	62.23	41.91	68.70	9.42
SRG-1MD	0.75	0.75	0.61	0.09	0.24	1456	460	184	48.0	40.16	65.84	42.43	69.55	5.34
SRG-1MD-A	0.75	0.75	0.61	0.09	0.24	1456	460	184	48.0	40.16	65.84	42.85	70.25	6.28
SRG-1MD-B	0.75	0.75	0.61	0.09	0.24	1456	460	184	48.0	40.16	65.84	39.21	64.28	2.42
SRG-2MD	0.53	0.53	0.42	0.10	0.21	1029	460	201	56.2	44.90	73.61	53.42	87.58	15.95

Table 8. Theoretical predictions according to ACI 440.2R. [2]

Test	$\varepsilon_{smax} = \varepsilon_{sd}$ [%]	ε_s [%]	ε_f [%]	ε'_f [%]	ε_c [%]	σ_s [MPa]	σ_f [MPa]	σ'_f [MPa]	y_c [MPa]	*theoretical* M_{max} [kN m]	*theoretical* F_{max} [kN]	*experimental* M_{max} [kN m]	*experimental* F_{max} [kN]	E_{rr} (%)
US	–	–	–	–	–	–	460	77	33.1	27.82	45.61	27.59	45.23	0.83
SRP-1LD	1.25	1.25	1.02	0.07	0.31	2417	460	154	39.5	34.75	56.97	34.95	57.30	0.58
SRP-1MD	0.72	0.72	0.58	0.09	0.23	1390	460	177	48.1	39.59	64.89	44.62	73.15	11.29
SRP-1HD	0.59	0.59	0.47	0.09	0.21	1135	460	186	52.6	42.05	68.94	56.79	93.10	25.95
SRG-1LD	1.25	1.25	1.02	0.07	0.31	2417	460	154	39.5	34.75	56.97	37.73	61.85	7.89
SRG-2LD	0.89	0.89	0.72	0.08	0.25	1709	460	168	44.3	37.50	61.47	41.91	68.70	10.53
SRG-1MD	0.72	0.72	0.58	0.09	0.23	1390	460	177	48.1	39.59	64.89	42.43	69.55	6.69
SRG-1MD-A	0.72	0.72	0.58	0.09	0.23	1390	460	177	48.1	39.59	64.89	42.85	70.25	7.62
SRG-1MD-B	0.72	0.72	0.58	0.09	0.23	1390	460	177	48.1	39.59	64.89	39.21	64.28	0.96
SRG-2MD	0.51	0.51	0.40	0.09	0.20	983	460	192	56.3	44.10	72.29	53.42	87.58	17.46

Figure

Click here to download Figure: Figures_June 4_2015.docx

Figure 1

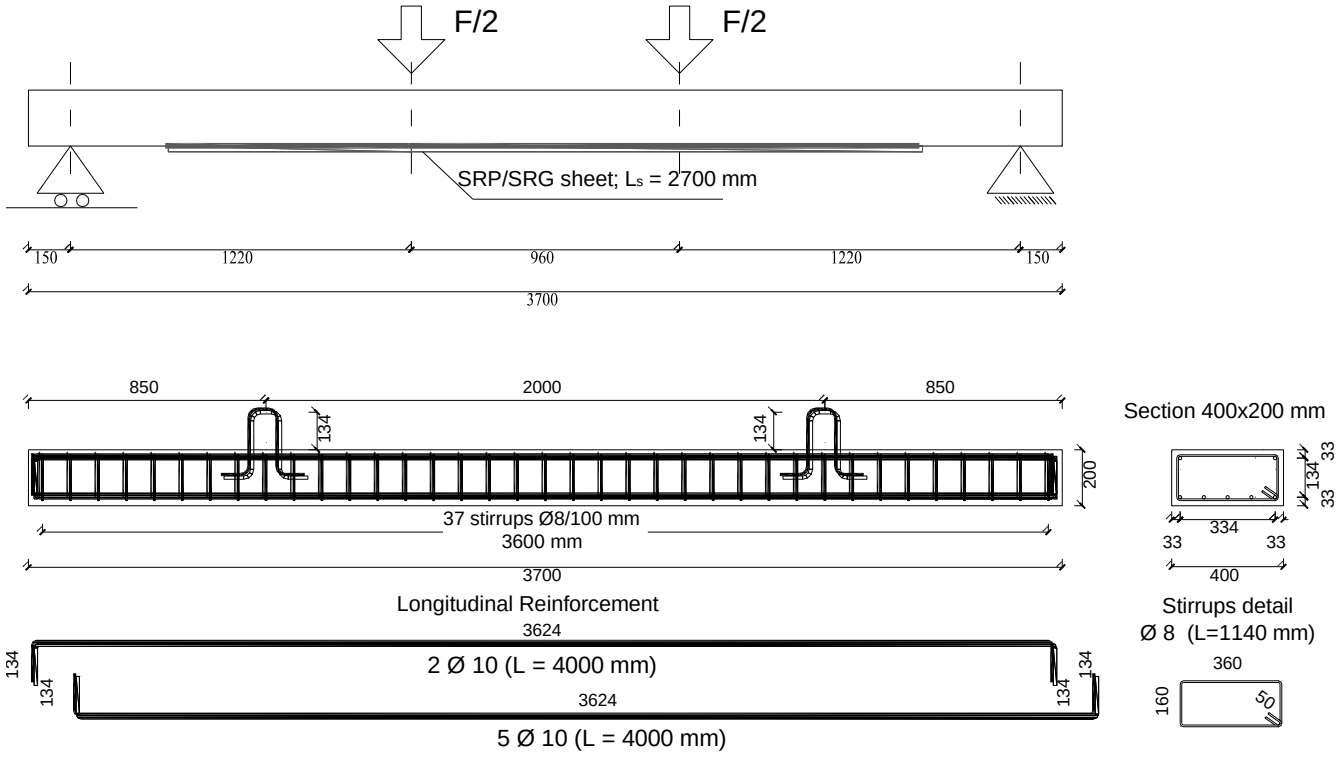

Figure 2

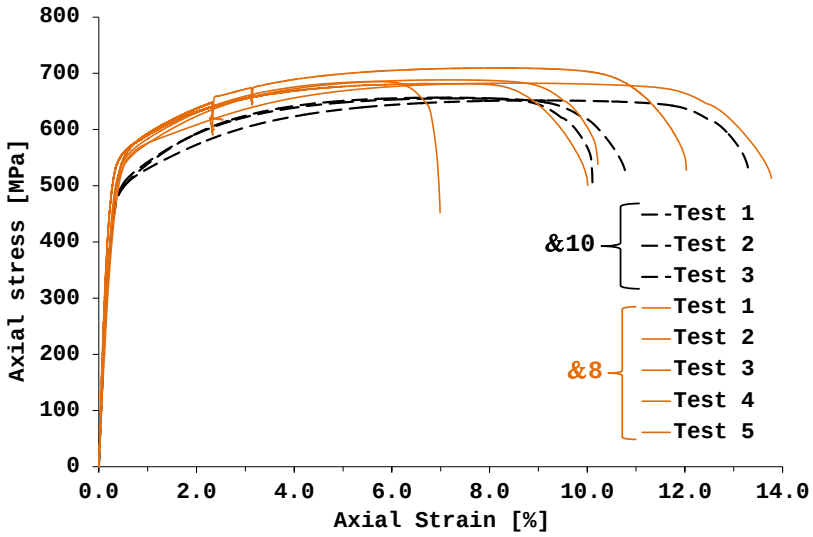
800
700
600
500
400
300
200
100
0
Axial stress [MPa]
0.0
2.0
4.0
6.0
8.0
10.0
12.0
14.0
Axial Strain [%]
&10
Test 1
Test 2
Test 3
&8
Test 1
Test 2
Test 3
Test 4
Test 5

Figure 3

Figure 4

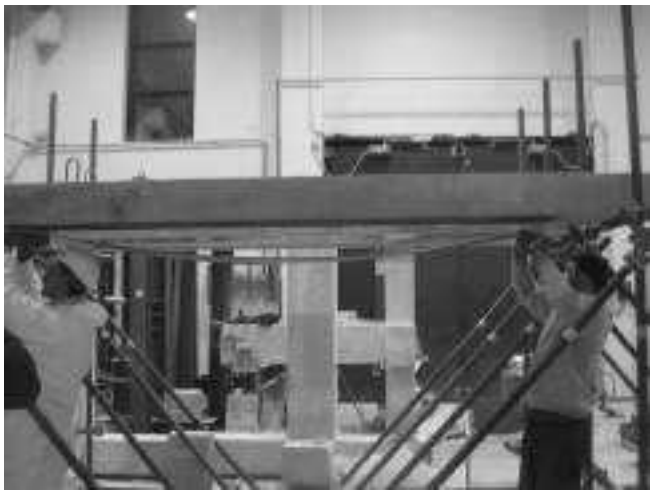

Figure 5 (only colour on the web)

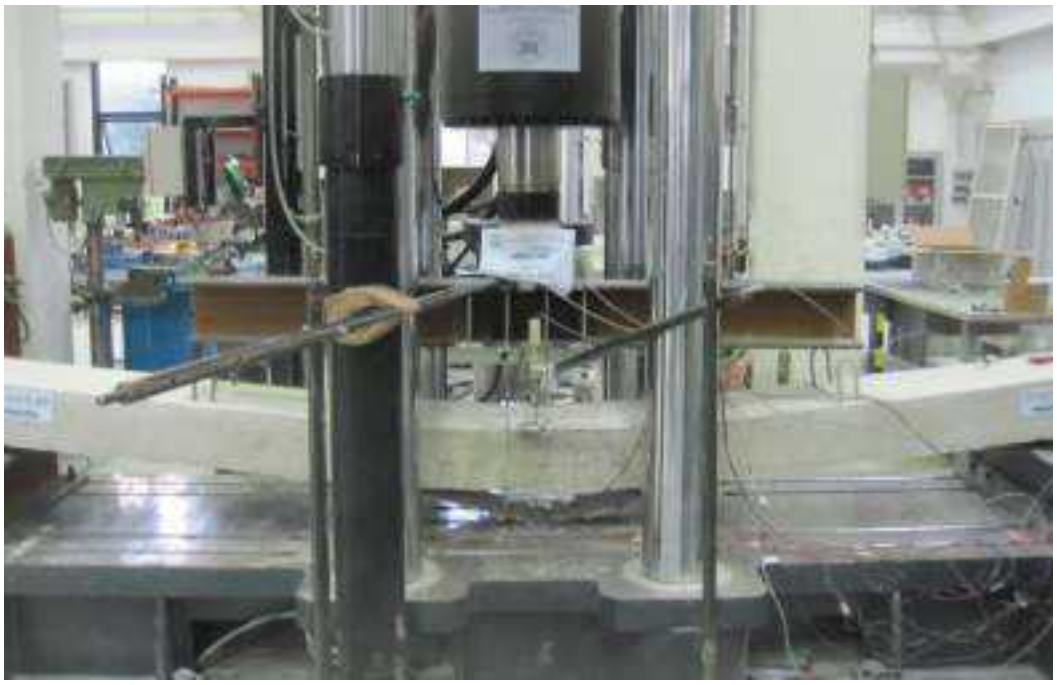

Figure 6 (only colour on the web)

FRONT VIEW

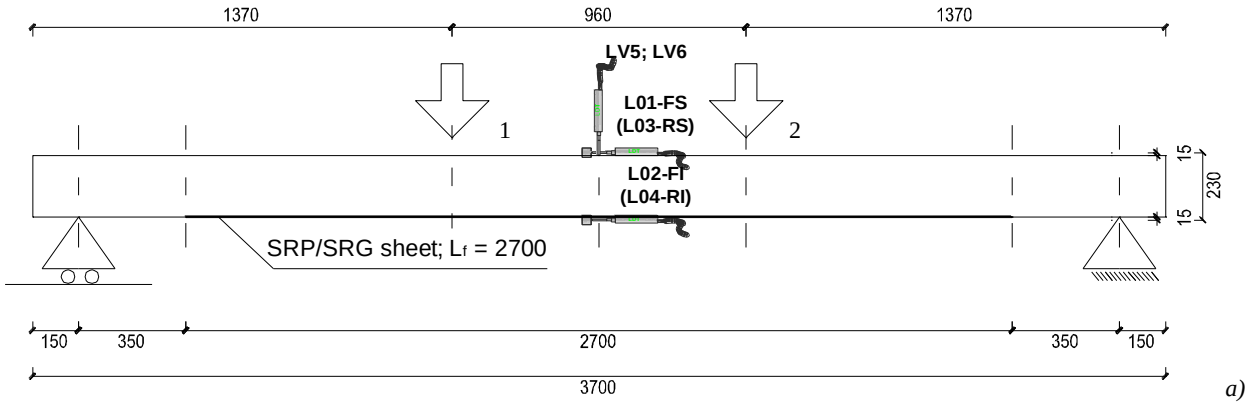

a)

TOP VIEW

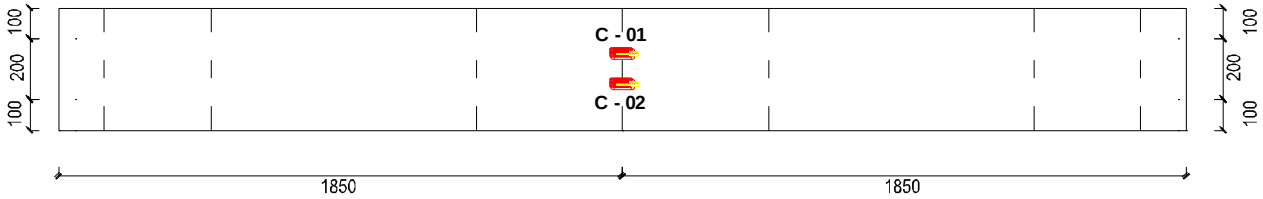

BOTTOM VIEW

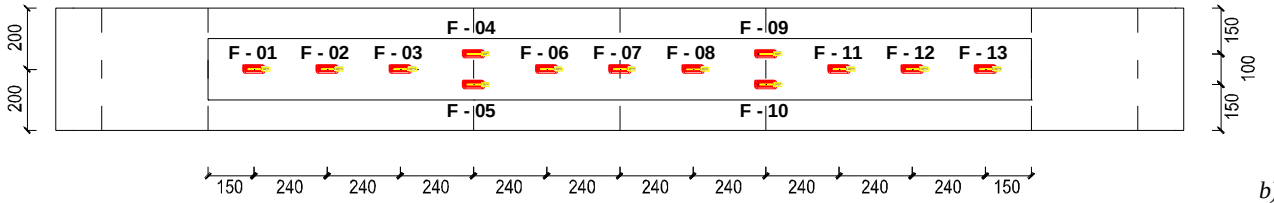

b)

Figure 7 (only colour on the web)

a) Test US

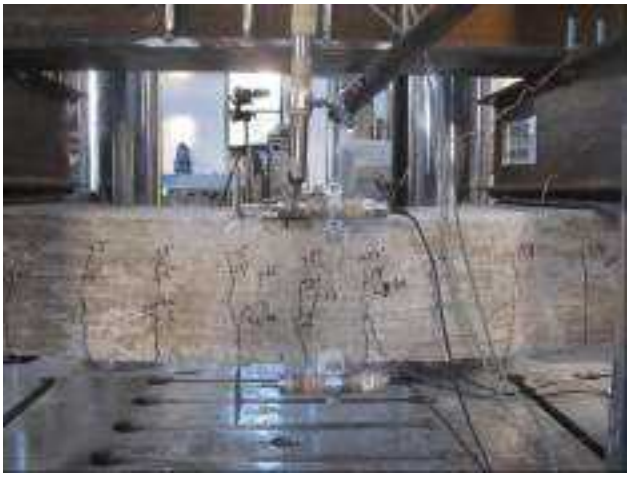


b) Test SRP-1LD


c) Test SRG-1LD


Figure 8 (only colour on the web)

a) Test SRP-1MD

b) Test SRG-1MD

c) Test SRG-1MD-A & SRG-1MD-B

Figure 9 (only colour on the web)

a) Test SRP-1HD

b) Test SRG-2LD & SRG 2MD

Figure 10 (only colour on the web)

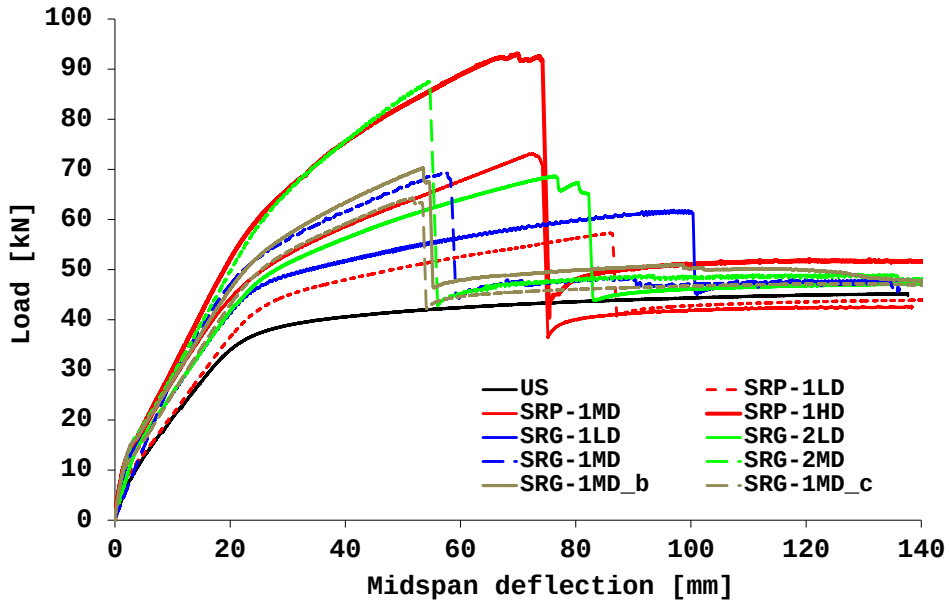

Figure 11 (only colour on the web)

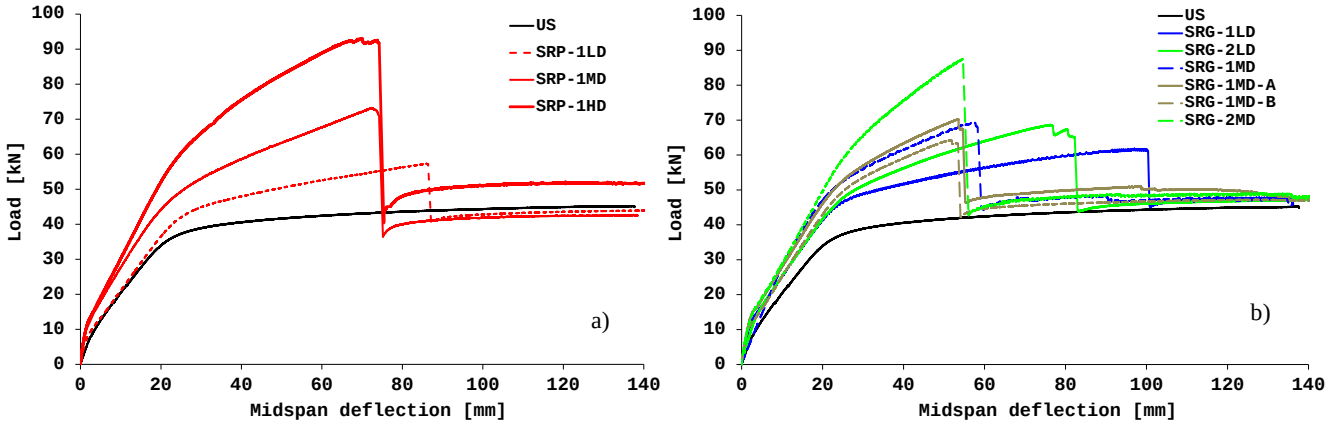

Figure 12 (only colour on the web)

Test SRP-1LD

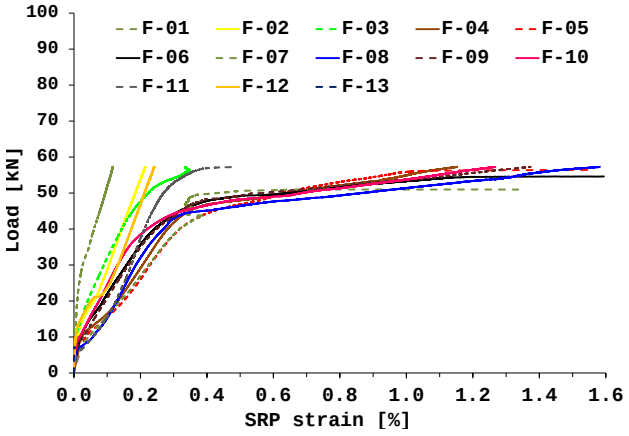

a)

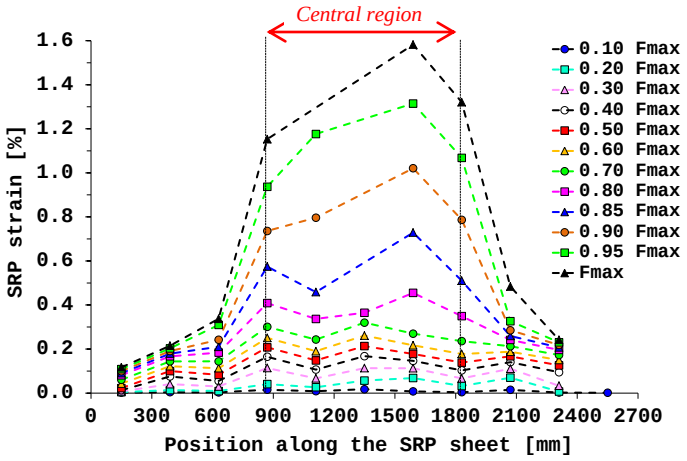

b)

Test SRG-1LD

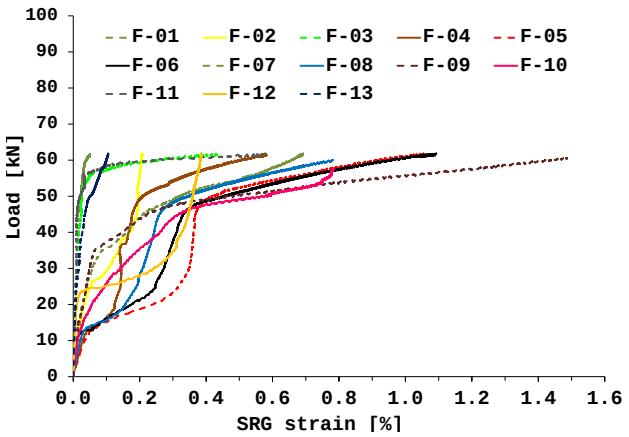

a)

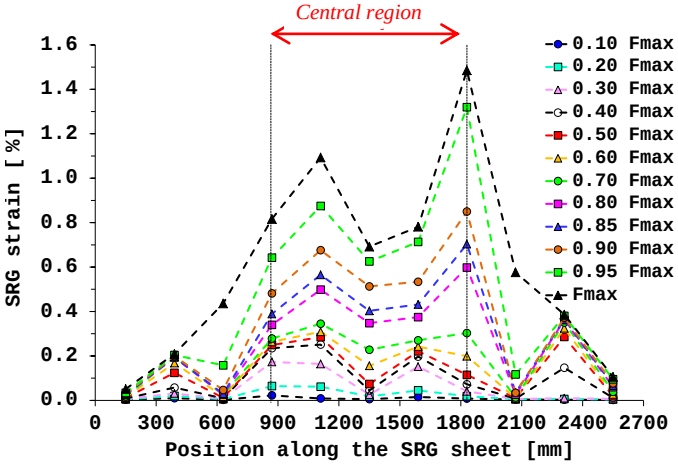

b)

Figure 13 (only colour on the web)

Test SRP-1MD

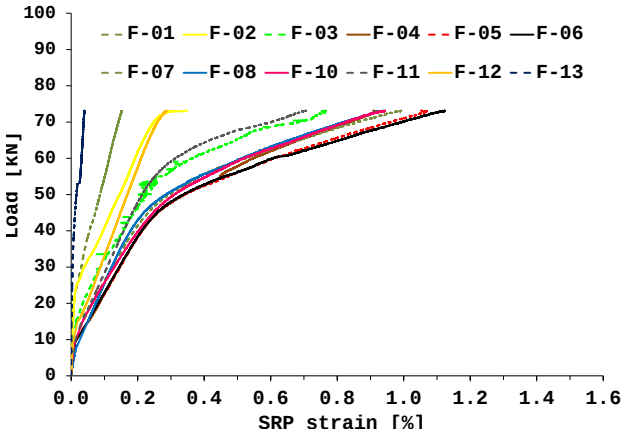

a)

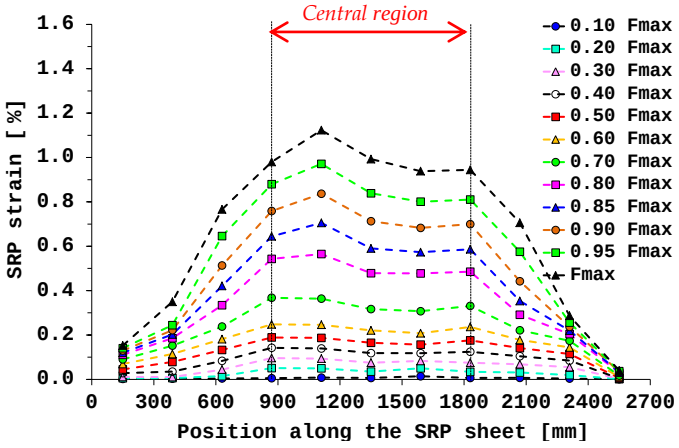

b)

Test SRG-1MD

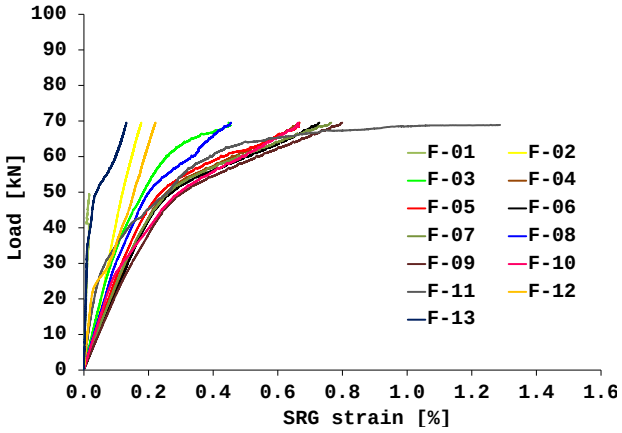

a)

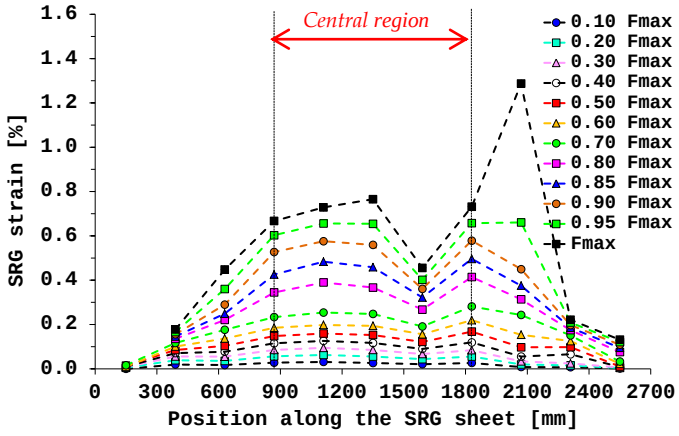

b)

Test SRG-1MD-A & SRG-1MD-B

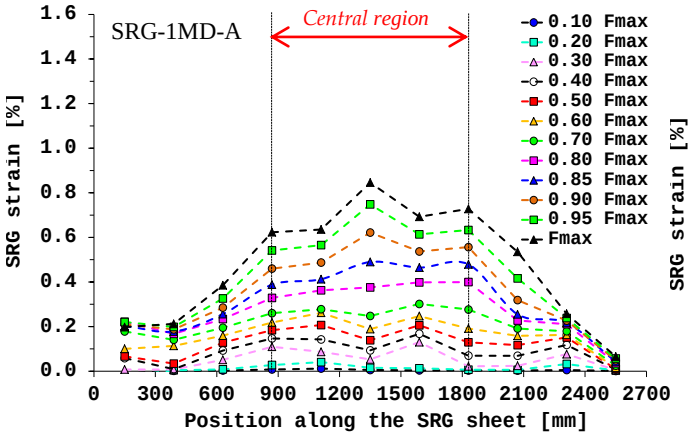

b)

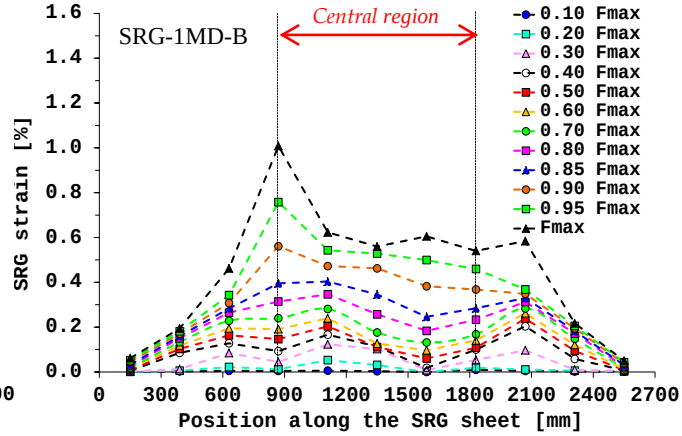

b)

Figure 14 (only colour on the web)

Test SRP-1HD

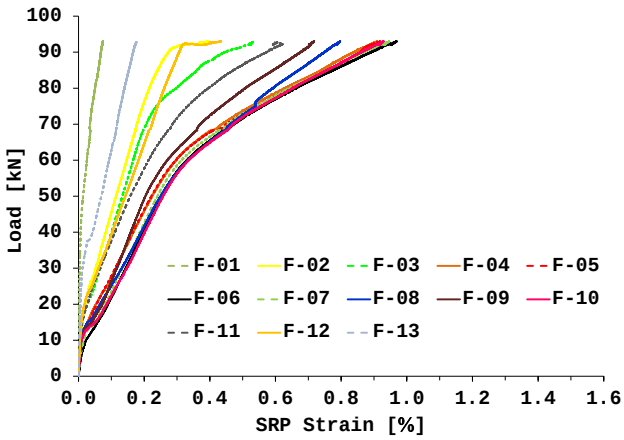

a)

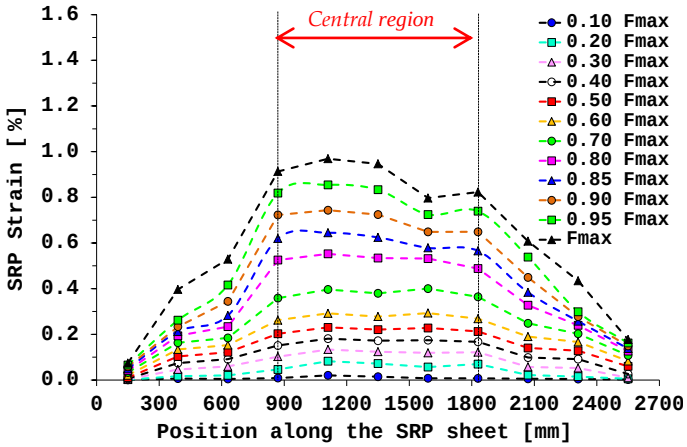

b)

Test SRG-2LD & SRG 2MD

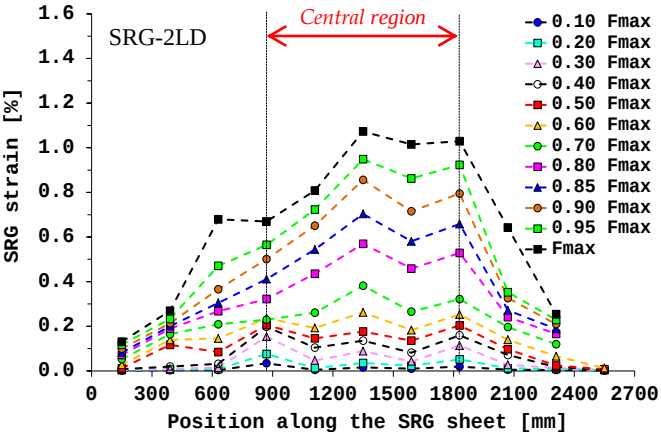

b)

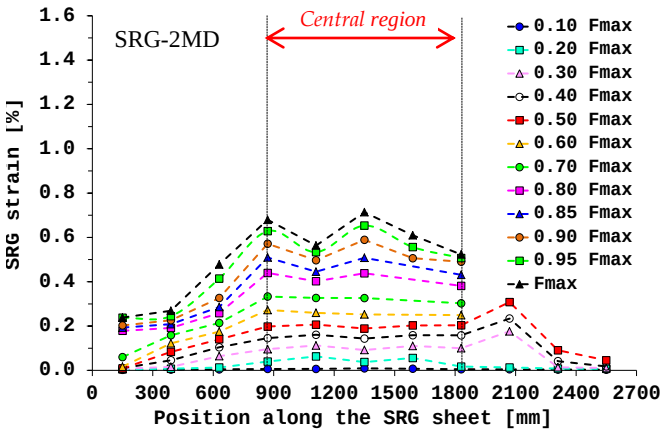

b)

Figure 15 (only colour on the web)

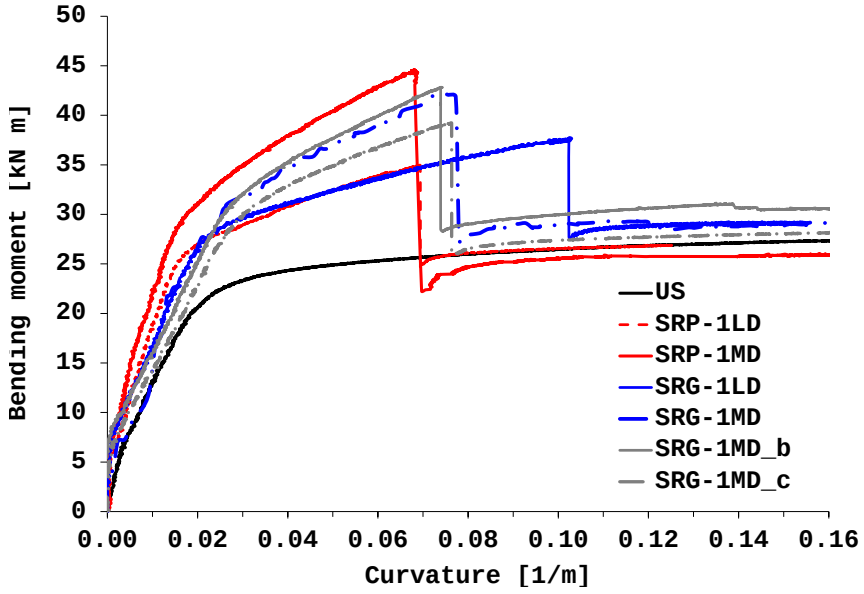

Figure 16 (only colour on the web)

Test SRP-1LD

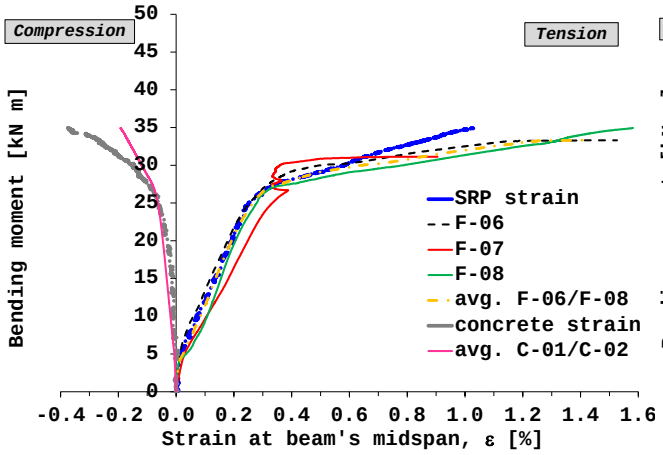

Test SRG-1LD

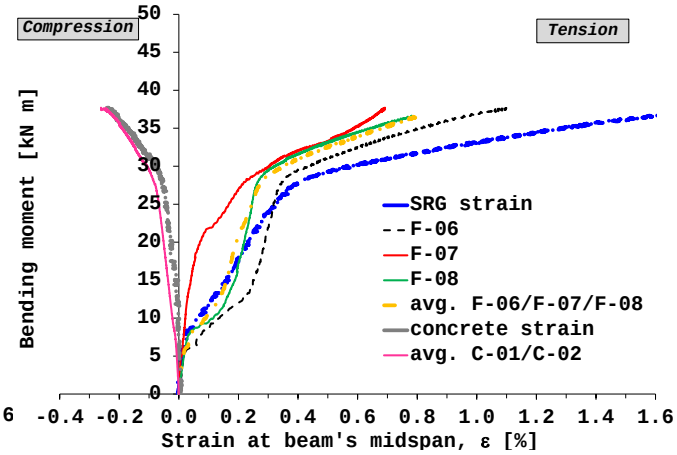

Test SRP-1MD

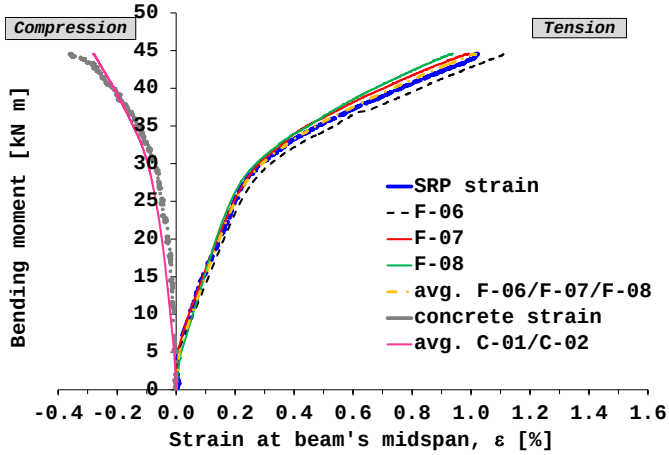

Test SRG-1MD

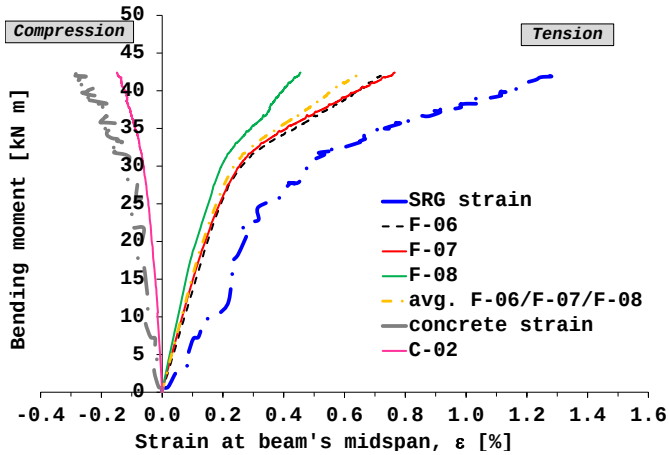

Test SRG-1MD-A

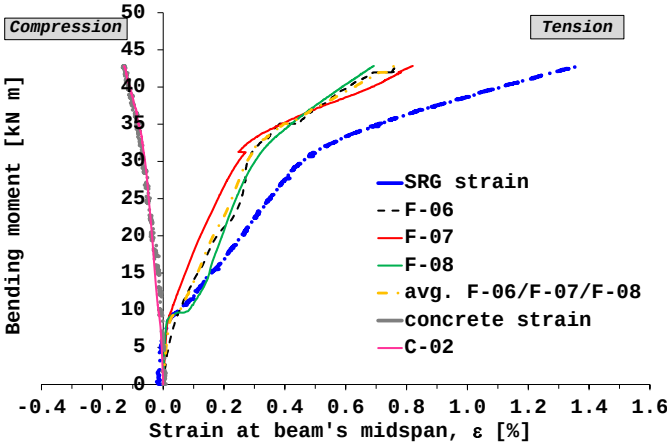

Test SRG-1MD-B

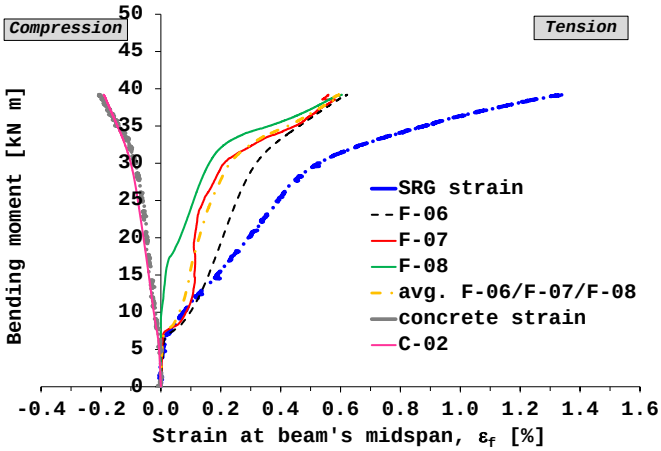

Figure 17 (only colour on the web)

Test SRP-1LD

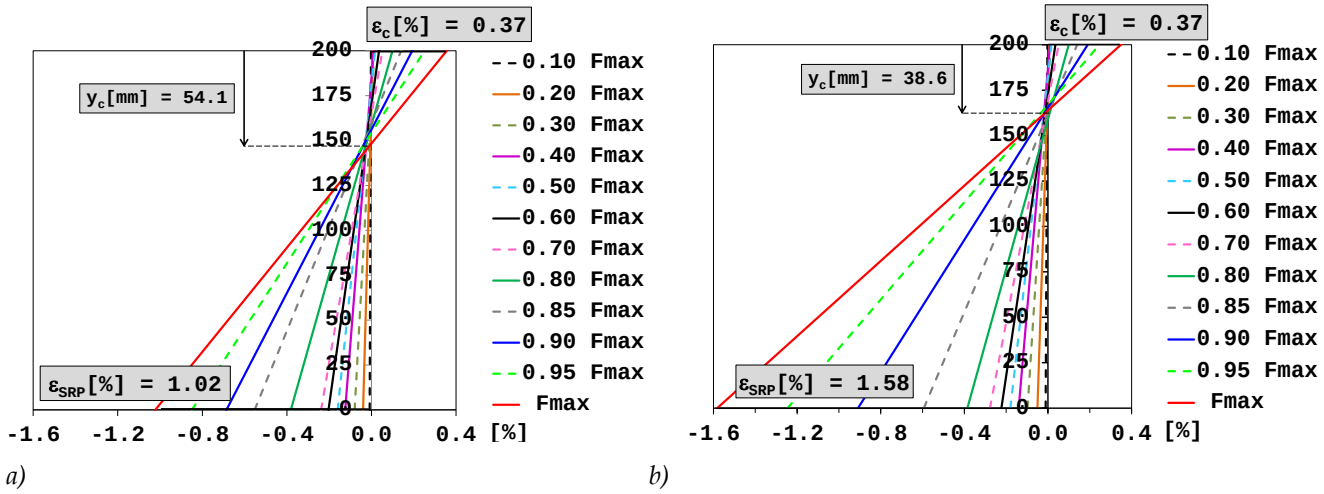

a) *b)*

Test SRG-1LD

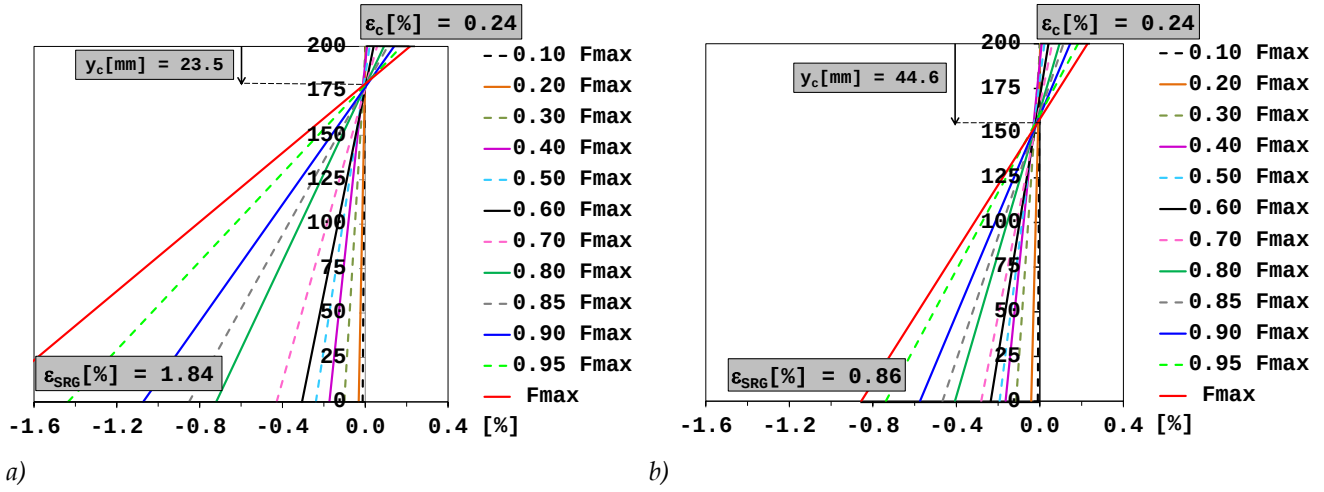

a) *b)*

Figure 18 (only colour on the web)

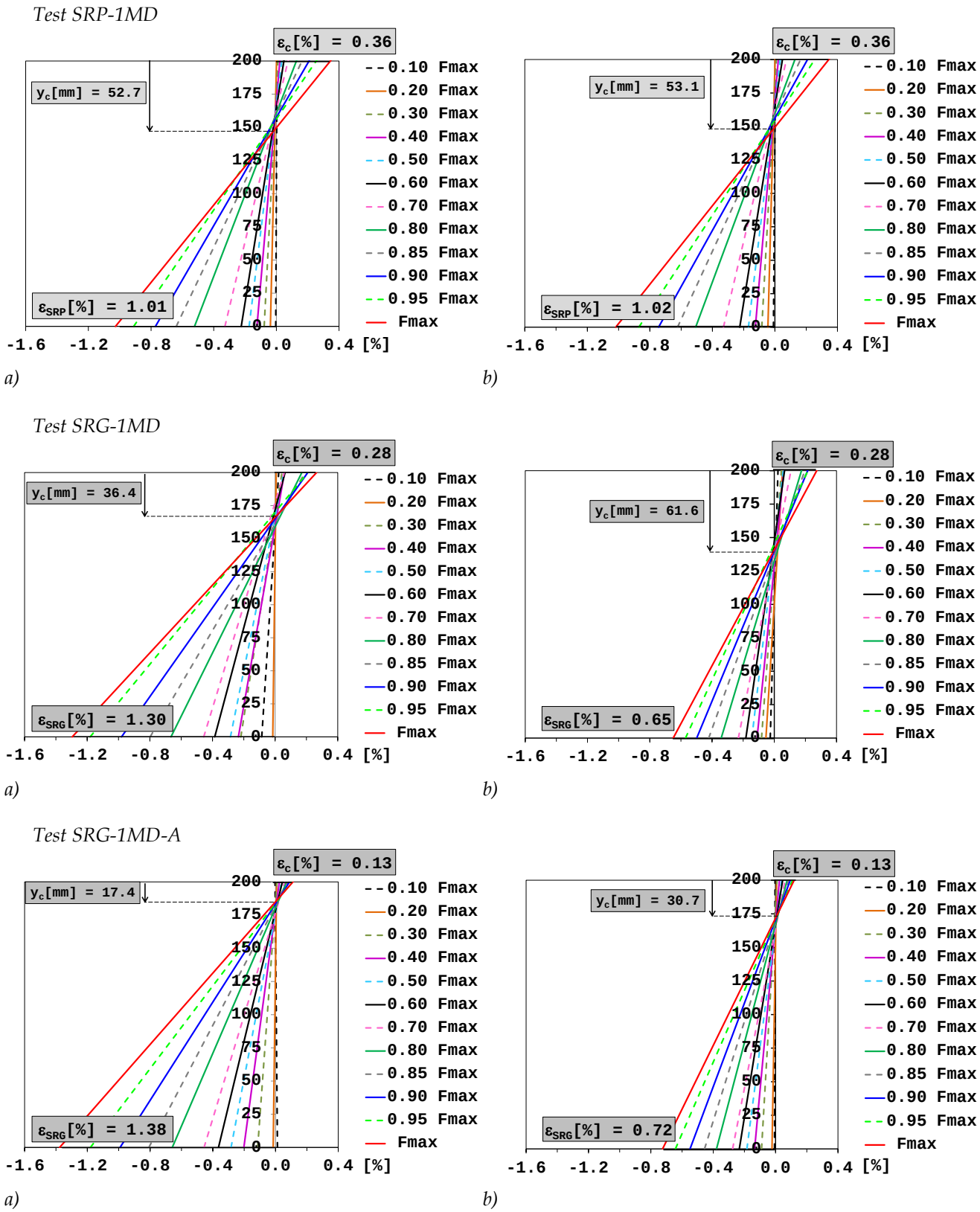

Figure 18 *(continued)*

Test SRG-1MD-B

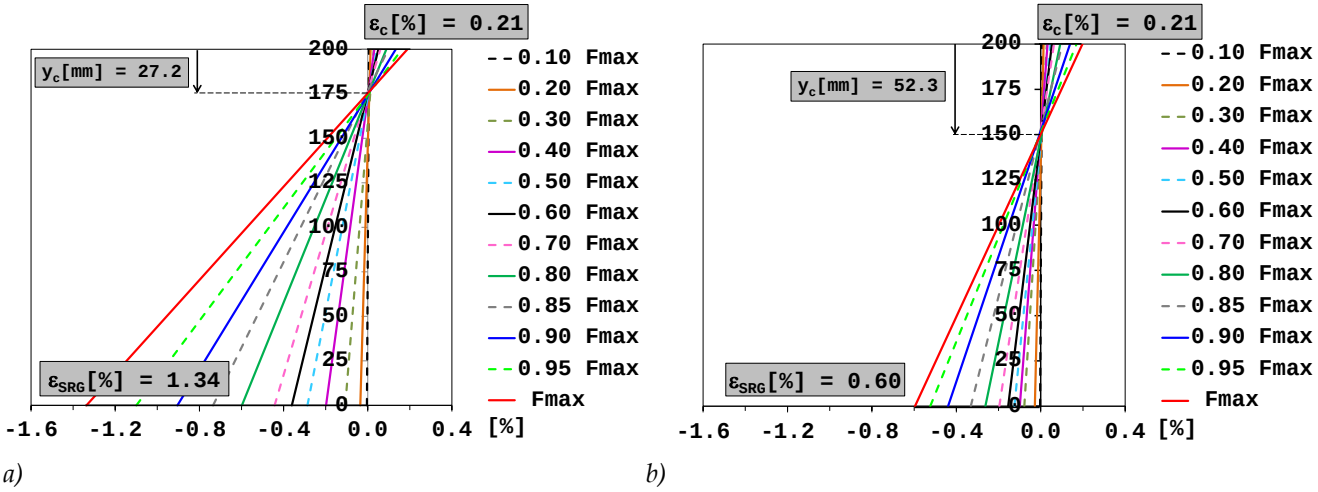

a) *b)*

Figure 19

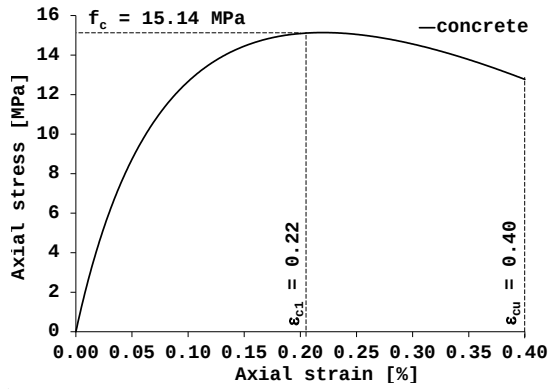

a)

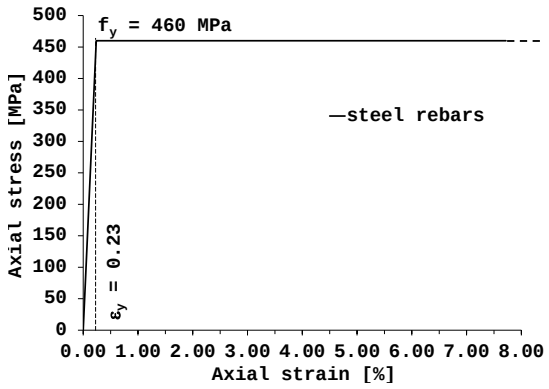

b)

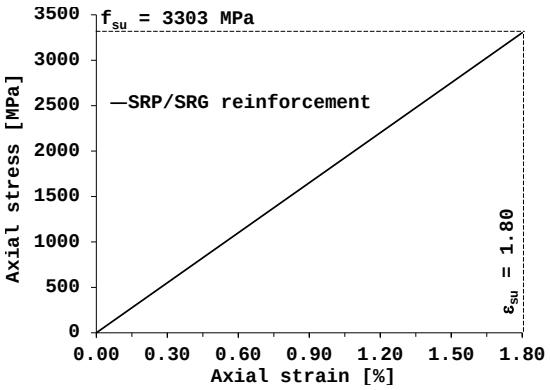

c)

Figure 20 (only colour on the web)

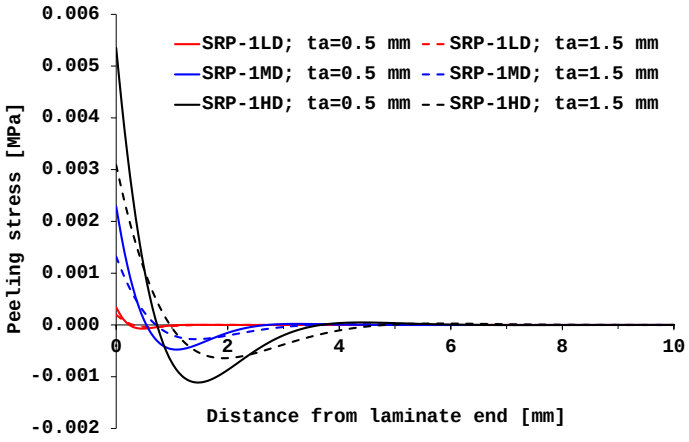

Figure 21 (only colour on the web)

Test SRP-1LD

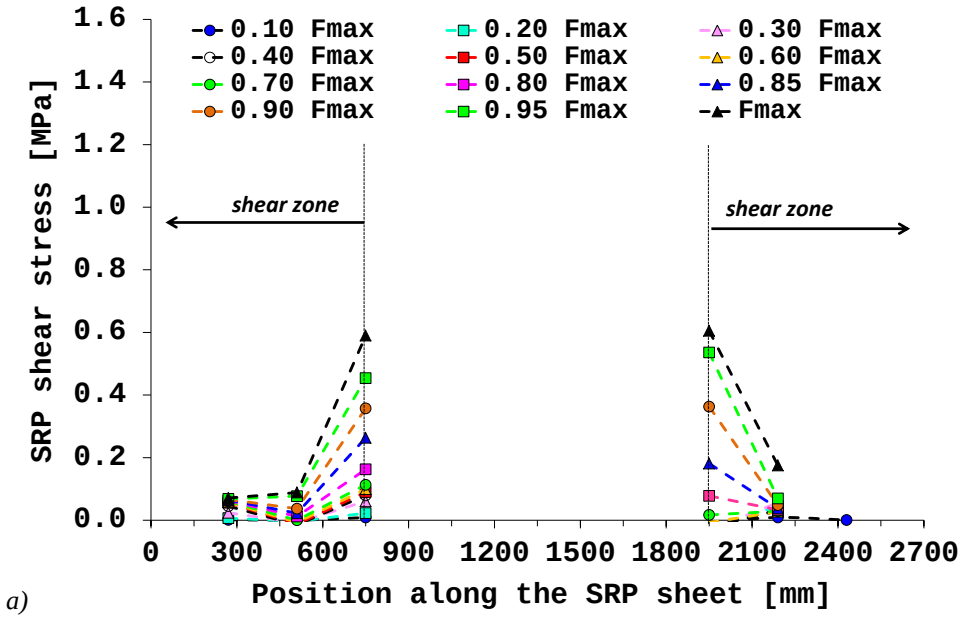

a)

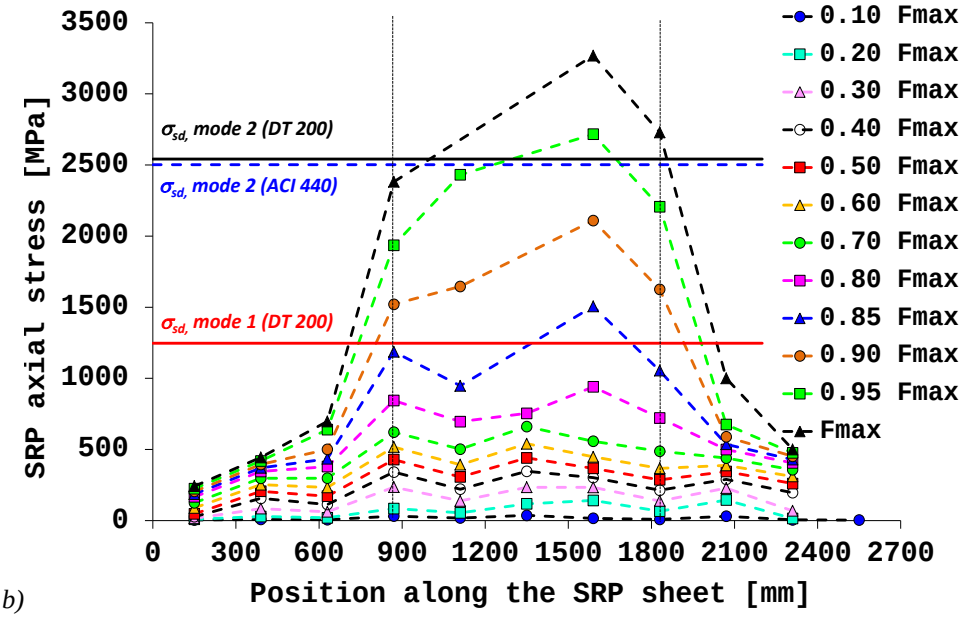

b)

Figure 22 (only colour on the web)

Test SRP-1MD

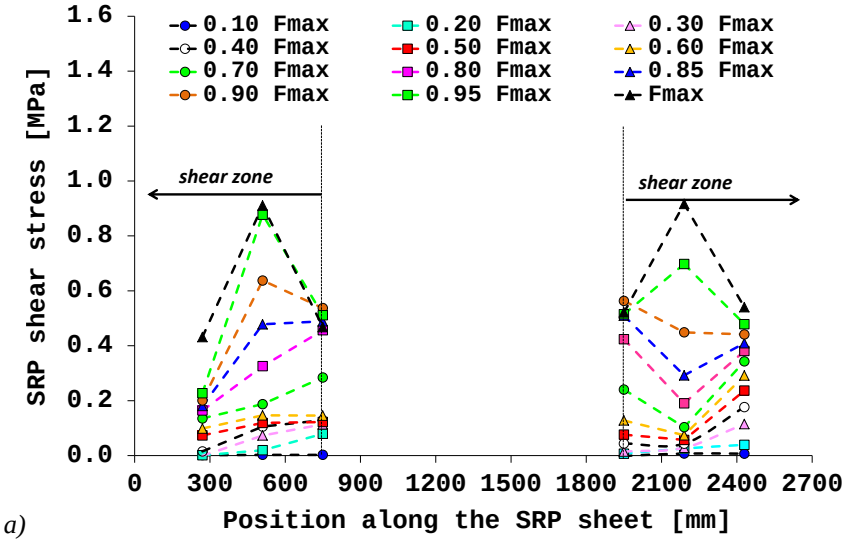

a)

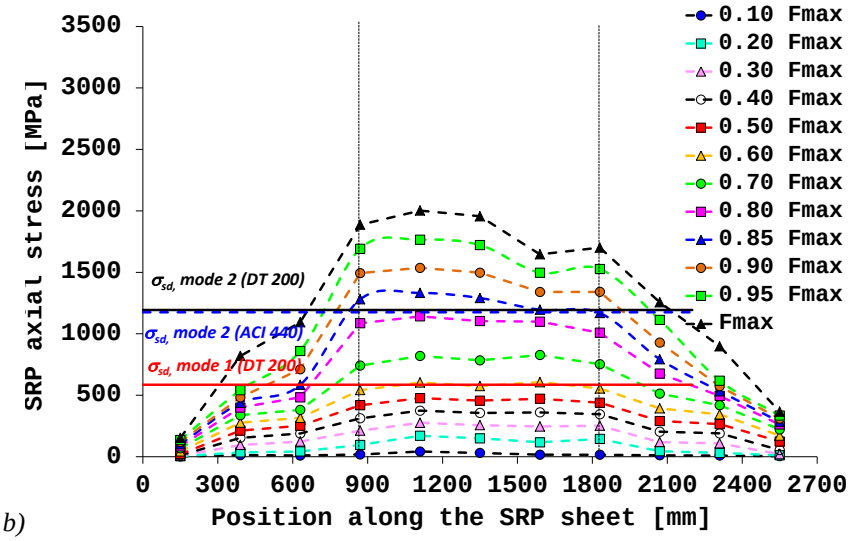

b)

Figure 23 (only colour on the web)

Test SRP-1HD

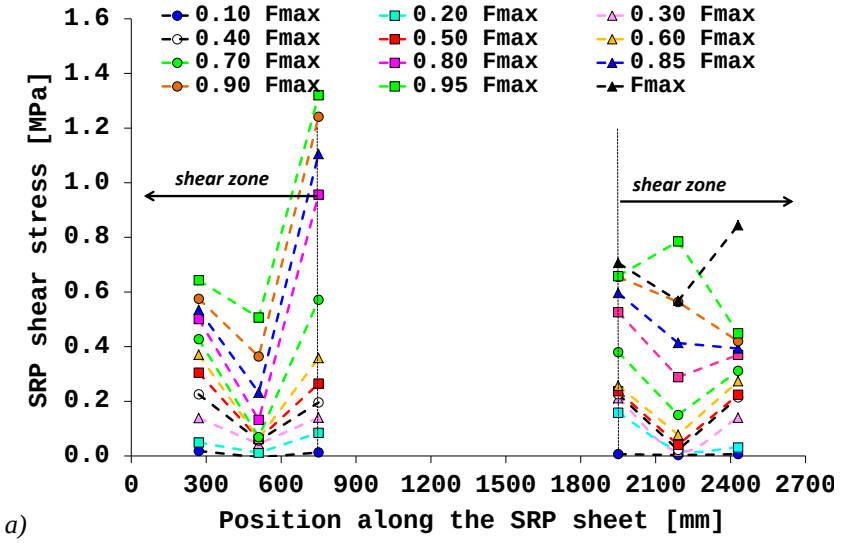

a)

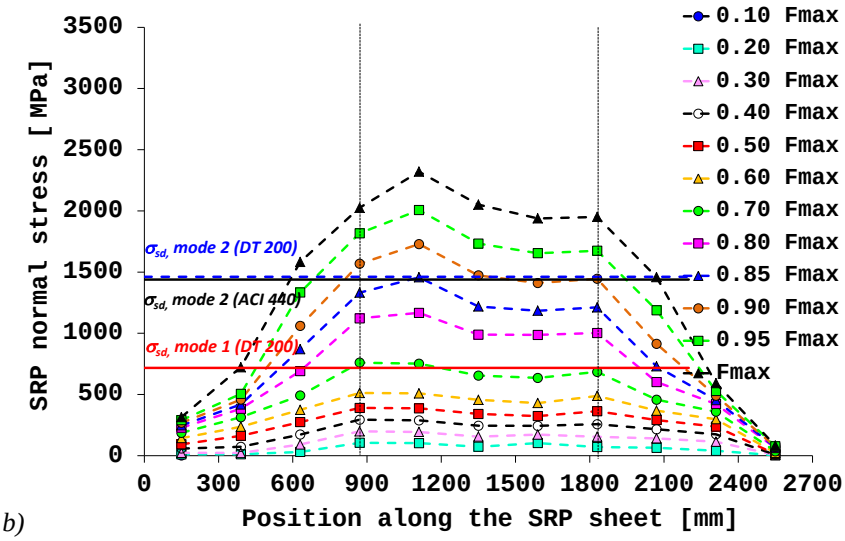

b)